

Structure of even-even Sr isotopes with $50 \leq N \leq 58$ neutrons

W. Urban,^{1,*} K. Sieja,² T. Rząca-Urban,¹ J. Wiśniewski,¹ A. Blanc,³ M. Jentschel,³ P. Mutti,³ U. Köster,³
T. Soldner,³ G. de France,⁴ G. S. Simpson,⁵ C. A. Ur,⁶ A. G. Smith,⁷ and J. P. Greene⁸

¹*Faculty of Physics, University of Warsaw, PL-02-093 Warsaw, Poland*

²*Université de Strasbourg, IPHC, Strasbourg, France and CNRS, UMR7178, 67037 Strasbourg, France*

³*Institut Laue-Langevin, 71 Av. des Martyrs, F-38000 Grenoble, France*

⁴*Grand Accélérateur National d'Ions Lourds (GANIL), CEA/DSM-CNRS/IN2P3, Boulevard Henri Becquerel,
Boîte Postale 55027, F-14076 Caen Cedex 5, France*

⁵*LPSC, Université Joseph Fourier Grenoble 1, CNRS/IN2P3, Institut National Polytechnique de Grenoble, F-38026 Grenoble Cedex, France*

⁶*INFN, Viale dell'Università, 2, 35020 Legnaro PD, Italy*

⁷*Department of Physics and Astronomy, The University of Manchester, M13 9PL Manchester, United Kingdom*

⁸*Argonne National Laboratory, Argonne, Illinois 60439, USA*

 (Received 4 August 2021; revised 27 August 2021; accepted 2 December 2021; published 13 December 2021)

Excited levels in ^{90}Sr , ^{92}Sr , ^{94}Sr , and ^{96}Sr nuclei were reinvestigated using high-statistics multiple- γ coincidence data from neutron-induced fission of ^{235}U and spontaneous fission of ^{252}Cf , measured using Exogam at Institut Laue Langevin and Gammasphere arrays, respectively. The experimental goal was the search for new excited levels and firm spin-parity assignments to known levels. A total of 23 new levels with 30 new or corrected decays and 39 new or improved spin-parity assignments were obtained in the four nuclei. Negative-parity structures on top of 3^- excitation were firmly identified and extended to higher spins. New positive-parity structures in ^{94}Sr and ^{96}Sr were observed with 3^+ excitations characteristic of γ collectivity. The 277.7-keV, $E2$ decay from the 1507.0-keV level to the *second* 0^+ level in ^{96}Sr , found in this paper, completes the coexisting deformed band in this nucleus. To learn about the microscopic structure of levels in the $^{88-96}\text{Sr}$ nuclei, we performed large-scale shell-model calculations. The calculations compared to the experiment, helped the discussion of the evolution of collectivity in strontium isotopes, highlighting the important role of various single-particle excitations in phase transitions and shape coexistence in the region. The special role of the neutron $9/2^+[404]$ extruder as a catalyst of the deformation change in the region is highlighted.

DOI: [10.1103/PhysRevC.104.064309](https://doi.org/10.1103/PhysRevC.104.064309)

I. INTRODUCTION

In a recent work [1], regular systematics of excitation energies of low-lying 0^+ levels in the neutron-rich nuclei of the mass $A \approx 100$ region were reported. Most of these levels follow smooth trends, but a few of them deviate from the pattern as shown in Fig. 6 of the work. The deviations are observed in Sr and Zr isotopes where the most pronounced and rapid shape-change phenomena in the region are observed. It is likely that the deviating levels are associated with coexisting shapes [2], and the observed deviations may provide an extra information on the shape evolution and coexistence in the region.

As illustrated in Fig. 1, the 0_2^+ excitations in Ru isotopes lower their energies with the increasing neutron number in a way suggesting strong interaction between 0_1^+ and 0_2^+ levels, pointing to a collective character of 0_2^+ levels [3]. In contrast, 0_2^+ excitations in Sr vary their energies in a way, which suggests very weak interaction between 0_1^+ and 0_2^+ levels. This weakness is dramatically highlighted by the 215.4-keV

excitation energy of the 0_2^+ level in ^{98}Sr [5], the lowest among 0_2^+ levels in all even-even nuclei. The proximity of 0_1^+ and 0_2^+ levels in ^{98}Sr with a well-deformed ground state, suggests that the 0_2^+ state has a different and rather noncollective nature.

It was proposed [1] that the $\nu 9/2[404]$ extruder orbital is involved in both, the rapid increase in the deformation in Sr and Zr isotopes at the neutron number $N \approx 59$ and the appearance of the 0_2^+ level at an extraordinary low excitation energy in ^{98}Sr and ^{100}Zr . This picture is backed by analogous observations around neutron number $N = 90$ in mass $A \approx 150$ region, another place where a sudden onset of deformation is observed. As shown in Refs. [6,7], it is the $\nu 11/2[505]$ extruder orbital, which is involved in the rapid increase of the deformation in the $A \approx 150$ region. The recent work [8] proposed, in addition, an involvement of the proton $9/2[404]$ extruder in the process and suggested that the action of extruder orbitals is not limited to passing of a single nucleon pair to a deformation-driving orbital (an effect proposed already at the advent of the Nilsson scheme [9]) but may be a multiple action. In this scenario, the upsloping extruder acts as a catalyst of the deformation process, crossing a number of deformation-driving down-sloping orbitals and passing and acquiring again pairs of nucleons as the Fermi level increases

*Corresponding author: urban@fuw.edu.pl

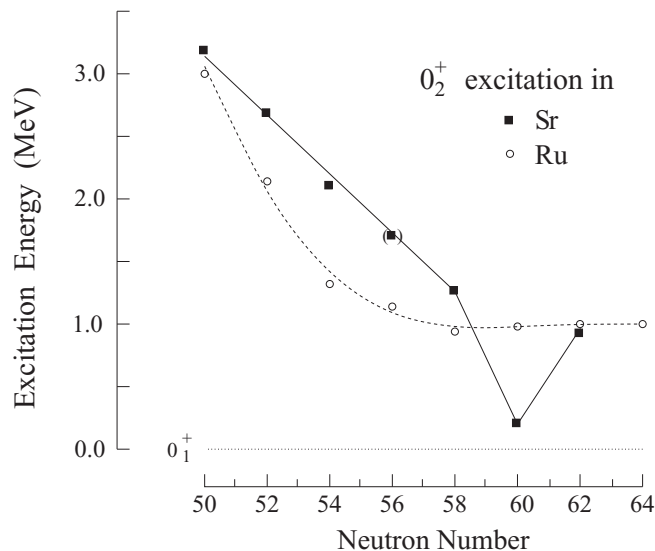


FIG. 1. Excitation energies of 0_2^+ levels in Sr (full squares) and Ru (open dots) isotopes. The data are taken from Refs. [3,4]. Lines are drawn to guide the eye.

with the increasing nucleon number. Such a multiple action has been considered theoretically within the “pair-hopping” model [10–12].

The two very different patterns of the deformation onset shown in Fig. 1 suggest that there is more than one mechanism involved in this process. As discussed in Refs. [12–17], the structure of transitional nuclei can be depicted as a “skeleton” of quasiparticle (q.p.) excitations in a self-consistent potential, “dressed” by various collective modes arising from both residual interactions between valence nucleons as well as from quantum fluctuations of the potential. There are also other quantum effects present in such nuclei, such as restoring broken symmetries of the potential through nuclear rotation or mixing coexisting configurations through quantum tunneling.

Uncovering these effects and mechanisms requires detailed knowledge of nuclear excitations in chains of isotopes and isotones and, above all, knowing their spins and parities, which are the fundamental quantum observable of nuclear systems in the laboratory frame. Such information helps tracing the characteristic excitations associated with various modes contributing to the development of collectivity in ground states as well as excited 0^+ configurations.

The purpose of the present paper is to update spectroscopic information on excited states in even Sr isotopes with $52 \leq N \leq 58$ in order to identify basic excitations building the 0^+ and other collective levels. Compared to our previous study of even-even Sr isotopes [18], based on the Eurogam measurement of prompt- γ radiation following spontaneous fission of ^{248}Cm [19], the present paper uses prompt- γ data of much higher statistics obtained from measurements of spontaneous fission of ^{252}Cf and neutron-induced fission of ^{235}U , respectively.

In Sec. II of the paper, the measurements and results are presented and compared with previous works with special emphasis on spin-parity assignments. In Sec. III, we present

TABLE I. Relative intensities of strong triple- γ cascades in Sr isotopes as observed in the Eurogam, Gammasphere, and EXILL measurements [18,20,21], respectively.

Isotope	Eurogam ^{248}Cm fission	Gammasphere ^{252}Cf fission	EXILL $^{235}\text{U} + n$ fission	Cascade (keV)
^{90}Sr	0.005	0.20	1.0	831-824-1271
	0.003	0.16	1.0	831-824-2128
	0.007	0.17	1.0	831-824-314
^{92}Sr	0.075	0.24	1.0	815-859-1093
	0.050	0.32	1.0	815-1371-581
^{94}Sr	0.13	0.22	1.0	837-1309-1010
	0.14	0.29	1.0	837-1089-678
^{96}Sr	0.35	0.47	1.0	815-978-674
	0.36	0.45	1.0	815-978-993

a phenomenological description of the results and use the large-scale shell-model (LSSM) calculations to identify various excitation modes and trace their evolution in Sr isotopes. Section IV provides the summary and the outlook.

II. MEASUREMENTS AND RESULTS

New experimental results on ^{90}Sr , ^{92}Sr , ^{94}Sr , and ^{96}Sr nuclei were obtained from measurements of γ rays following spontaneous fission of ^{252}Cf and neutron-induced fission of ^{235}U , performed using the Gammasphere [20] and the Exogam at Institut Laue Langevin (EXILL) [21] arrays of anti-Compton Spectrometers, respectively. The two experiments provided significantly higher number of triple- γ coincidences, compared to the Eurogam study [18], especially for $^{90,92}\text{Sr}$ isotopes. Relative intensities of strong triple- γ cascades as seen in the Eurogam, Gammasphere, and EXILL measurements are presented in Table I. The present paper is based predominantly on the EXILL data with the Gammasphere data used as a countercheck.

The present paper focuses on two experimental aspects, the identification of key, collective excitations mentioned in the Introduction and reliable spin-parity assignments. The assignments are helped by new angular-correlation techniques for the EXILL [21] and ^{252}Cf fission data [22] as well as new techniques for directional-polarization correlations using EXILL [23].

A. Excitations in ^{90}Sr

Low-spin levels of ^{90}Sr were studied before in the β^- decay of the 0^- ground state and the 3^- isomer of ^{90}Rb [24]. Medium-spin excitations were studied in heavy-ion-induced reactions [25,26]. In the present paper, we observe weak prompt- γ population of ^{90}Sr levels in the neutron-induced fission (not competitive to Refs. [25,26]) and a strong population in the β^- decay of ^{90}Rb , produced either in fission or in β^- decay of its isobars. Our triple-coincidence analysis provides results competitive to Ref. [24], and we confirm most of the levels with spin $I \leq 5$ listed in the compilation [27]. The quality of the coincidence data from EXILL is illustrated

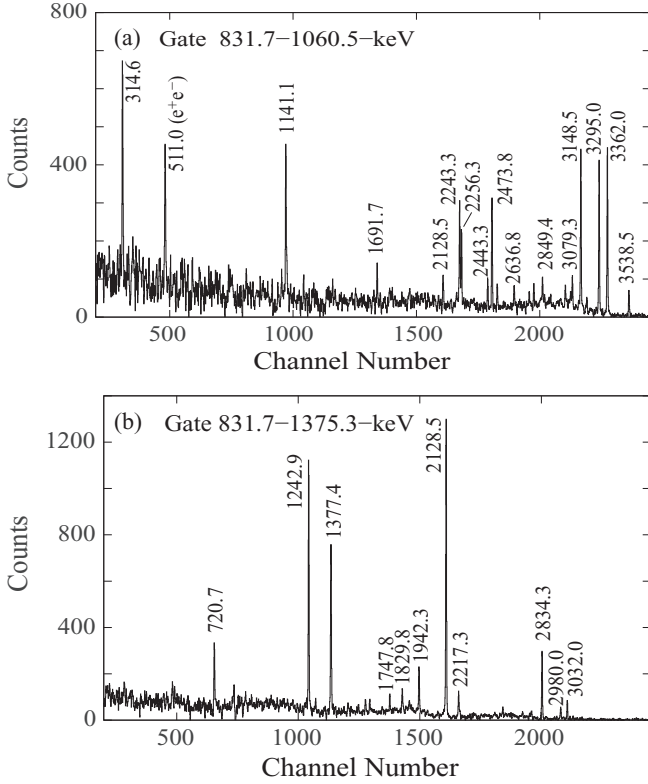


FIG. 2. Coincidence γ spectra doubly gated on lines of ^{90}Sr as observed in the present paper. Some known lines of ^{90}Sr [24] seen in the figure are not listed in Table II.

in Fig. 2, which shows examples of γ spectra doubly gated on strong lines of ^{90}Sr .

Table II lists all known levels in ^{90}Sr up to of 3 MeV and those high-energy levels where new information was obtained in this paper. Only transitions and decay branching, which are observed in coincidence spectra gated above the level in question, are shown. New results are marked in Table II with asterisks.

Spins and parities of levels in ^{90}Sr are obtained from angular-correlation and directional-polarization-correlation measurements performed using EXILL. The results are listed in Tables III and IV, respectively. All results in Table IV are new.

Figure 3 shows the partial excitation scheme of ^{90}Sr . Only levels and transitions discussed in the text are shown.

Spins and parities of 831.70-, 1655.95-, 1892.3-, and 2497.3-keV levels reported in the compilation [27] are confirmed. We note the significantly higher 2497.4 keV branching from the 2497.3-keV level. The level at 2586(1) keV reported in Ref. [27] is not observed in the present paper.

For the 2207.0-keV level, we assign spin-parity 3^- . The χ^2 -test value for this assignment is an order of magnitude smaller than for the 2^+ spin-parity hypothesis. Very weak decays between this level and other negative-parity levels (see Refs. [25,26]) suggest different structures.

For the 2528.1-keV level, we assign positive parity. The 3^- hypothesis [27] is not confirmed, coinciding with the lack of

TABLE II. Energies E_i and spin-parities I_i^π of excited states in ^{90}Sr with energies E_γ and γ -ray branching ratios I_γ for γ decays as observed in this paper. Levels and decays which are new or differ from the compilation [27] are marked with an asterisk. E_f and I_f^π denote the energy and spin-parity of levels populated by γ decays listed in the third column.

E_i (keV)	I_i^π	E_γ (keV)	I_γ (rel.)	E_f (keV)	I_f^π
831.70(5)	2^+	831.70(5)		0.0	0^+
1655.95(8)	4^+	824.25(5)			2^+
1892.3(1)	2^+	1060.50(5)	100(3)	831.70	2^+
		1892.5(3)	8(1)	0.0	0^+
2207.0(1)	3^- *	314.6(1)	5.1(7)	1892.3	2^+
		551.2(2)	4.9(7)	1655.95	4^+
		1375.30(5)	100(3)	831.70	2^+
2497.3(1)	(2^+)	1665.60(5)	100(3)	831.70	2^+
		2497.4(1)	49(5) *	0.0	0^+
2528.1(2)	$3^+, 4^+$ *	872.4(1)	55(15)	1655.95	4^+
		1696.2(1)	100(10)	831.70	2^+
2571.0(2)	$3^{(+)}$ *	1739.3(1)		831.70	2^+
2673.8(4)	0^+ *	1842.1(3)		831.70	2^+
2927.7(1)	$4^{(-)}$	720.7(1)	15(5) *	2207.0	3^-
		1271.7(1)	100(5)	1655.95	4^+
2971.1(2)	0^+	2139.4(1)		831.70	2^+
3449.8(1)	2^+ *	952.7(1)		2497.3	(2^+)
		1242.90(5)		2207.0	3^-
		1793.9(1)		1665.95	4^+
		2617.7(3)		831.70	2^+
3584.5(1)	3^+ *	1377.4(2)		2207.0	3^-
		2752.80(5)		831.70	2^+
4036.2(2)	$2^{(+)}$ *	3204.5(1)		831.70	2^+
4135.3(2)	$1, 2^+$	3303.6(1)		831.70	2^+
4148.8(1)	3^+ *	1941.9(1)		2207.0	3^-
		2256.3(2)		1892.3	2^+
		3317.05(5)		831.70	2^+
4335.4(2)	3^+ *	3503.6(1)		831.70	2^+
		2128.5(1)		2207.0	3^-
4366.1(2)	1^+ *	3534.4(1) *		831.70	2^+
		2473.8(1)		1892.3	2^+
4404.5(3)	$2, 3$ *	3572.8(2)		831.70	2^+
5430.6(3) *		3538.5(2)		1892.3	2^+
		4598.6(3)		831.7	2^+

decays from 4^- and 5^- levels [25,26]. The 3^+ assignment fits best the data, but the 4^+ is also possible.

For the 2571.0-keV level, we assign spin-parity $I=3^{(+)}$. The large mixing ratio $\delta=8.9$ fits better the angular-correlation data than the other solution with $\delta=-0.06$.

The 1842.1-keV decay of the 2673.8-keV level is confirmed. Angular correlations support the 0^+ spin-parity assignment to this level [27] because of the very large A_4/A_0 value, the unique feature of a 0-2-0 cascade.

The 2927.7-keV level has spin $I=4$, the only value consistent with angular correlations for both transitions depopulating this level and their branching. No decay to the 2^+ level at 831.70 keV favors negative parity.

Our angular correlation data support the 0^+ spin-parity of the 2971.1-keV level [27].

TABLE III. Angular correlation coefficients for γ - γ cascades in ^{90}Sr populated in neutron-induced fission of ^{235}U . The label “sum” denotes summed correlations with all quadrupole transitions below $E_{\gamma 1}$.

$E_{\gamma 1}-E_{\gamma 2}$ cascade	A_2/A_0 expt.	A_4/A_0 expt.	Spins in cascade	$\delta_{\text{exp}}(\gamma 1)$
824.25-831.70	0.102(9)	0.029(42)	4-2-0	
1060.50-831.70	-0.069(11)	0.061(29)	2-2-0	0.44(2)
			3-2-0	0.003(16)
1375.30-831.70	-0.129(14)	0.014(27)	3-2-0	-0.07(3)
			2-2-0	0.53(2)
1665.6-831.70	0.249(31)	0.012(72)	2-2-0	0.002(44)
			3-2-0	0.7(+6,-2)
1696.2-831.70	0.095(85)	-0.112(95)	3-2-0	2.4 (4)
1739.3-831.70	-0.115(40)	-0.087(80)	3-2-0	8.9(29)
				or -0.06(5)
1842.1-831.70	-0.17(2)	1.02(24)	0-2-0	
2139.4-831.70	0.32(5)	0.88(4)	0-2-0	
2752.80-831.70	0.215(15)	-0.023(34)	2-2-0	0.05(2)
			3-2-0	0.50(5)
				or 1.36(12)
3204.5-831.70	0.012(66)	0.39(14)	2-2-0	-9(4)
3303.6-831.70	-0.169(35)	0.01(7)	1-2-0	-0.07(3)
			2-2-0	0.60(8)
3317.05-831.70	0.243(11)	0.006(26)	2-2-0	0.009(16)
			3-2-0	0.62(7)
3503.6-831.70	0.298(39)	0.01(10)	2-2-0	-0.07(6)
			3-2-0	0.83(26)
3534.4-831.70	-0.204(13)	-0.018(27)	1-2-0	0.04(1)
			3-2-0	-0.17(2)
3572.8-831.70	0.239(66)	0.24(15)	2-2-0	-2.3(5)
			3-2-0	0.6(2)
2128.5-1375.30	0.84(30)	0.06(6)	3-3-2	0.7(1)
				or -18(10)
1271.7-sum	0.073(38)	-0.12(9)	4-2-0	0.3(1)
1793.9-sum	0.08(5)	0.22(12)	2-2-0	-4.9(12)

TABLE IV. Experimental $P_{\text{exp}}(\gamma 1)$ and theoretical $P_{\text{th}}(\gamma 1)$ values of linear polarization for the $\gamma 1$ (upper) transition in a γ - γ cascade of ^{90}Sr as obtained from directional-polarization correlations in this paper. The correlating 831.70-keV $\gamma 2$ is assumed to be a $\Delta I=2$, E2 with $\delta=0$.

$E_{\gamma 1}-E_{\gamma 2}$	$P_{\text{exp}}(\gamma 1)$	Spin parity	$\delta_{\text{exp}}(\gamma 1)$	$P_{\text{th}}(\gamma 1)$
1060.50-831.70	0.34(7)	2 ⁺ -2 ⁺ -0 ⁺	0.44(2)	0.439(3)
		3 ⁻ -2 ⁺ -0 ⁺	0.003(16)	0.105(6)
1375.30-831.70	0.090(68)	3 ⁻ -2 ⁺ -0 ⁺	-0.07(3)	-0.076(7)
		2 ⁺ -2 ⁺ -0 ⁺	0.53(2)	0.426(3)
1665.60-831.70	0.14(17)	2 ⁺ -2 ⁺ -0 ⁺	0.002(44)	0.429(9)
		3 ⁻ -2 ⁺ -0 ⁺	0.7(+6,-2)	-0.43(9)
2752.80-831.70	-0.38(16)	2 ⁻ -2 ⁺ -0 ⁺	0.05(2)	-0.430(4)
		3 ⁺ -2 ⁺ -0 ⁺	0.50(5)	-0.354(6)
3317.75-831.70	-0.50(15)	2 ⁻ -2 ⁺ -0 ⁺	0.009(16)	-0.439(6)
		3 ⁺ -2 ⁺ -0 ⁺	0.62(7)	-0.404(7)
3503.6-831.70	-0.60(45)	2 ⁻ -2 ⁺ -0 ⁺	-0.07(6)	-0.409(8)
		3 ⁺ -2 ⁺ -0 ⁺	0.83(26)	-0.468(9)
3534.4-831.70	-0.19(17)	1 ⁺ -2 ⁺ -0 ⁺	0.04(1)	-0.307(5)
		3 ⁺ -2 ⁺ -0 ⁺	-0.17(2)	-0.045(9)

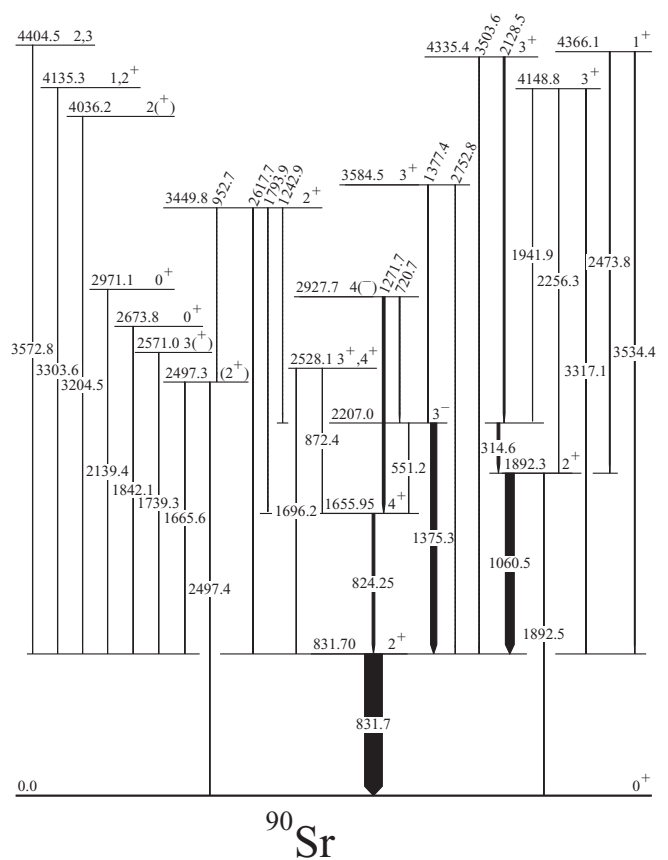


FIG. 3. Partial level scheme of ^{90}Sr as seen in this paper following fission of ^{235}U induced by thermal neutrons. Arrow width is proportional to the observed γ intensity.

Angular- and directional-polarization correlations for the 2752.8-831.7-keV cascade indicate spin-parity of 2⁻ or 3⁺ for the 3584.5-keV level. The log ft of 6.5 for this level, populated in the β^- decay of the 3⁻ isomer in ^{90}Rb [27] and the observed branching favor spin-parity 3⁺.

For the 3449.8-keV level, the present angular correlations uniquely indicate spin $I=2$. Positive parity is consistent with the log ft of 6.9 for this level, populated in the β^- decay of the 3⁻ isomer in ^{90}Rb [27] and the decay branching. Similarly, angular correlations uniquely indicate spin $I=2$ for the 4036.2-keV level. The decay branching for this level favors positive parity.

Angular correlations for the 3303.6-831.7-keV cascade are consistent with spin $I=1$ or $I=2$ for the 4135.3-keV level, also proposed in Ref. [27]. The large mixing ratio for the 2-2-0 hypothesis favors positive parity.

Angular and directional-polarization correlations for the new 3503.6-831.7-keV cascade indicate spin-parity 2⁻ or 3⁺ for the 4335.4-keV level. The log ft of 6.2 for this level, populated in the β^- decay of the 3⁻ isomer in ^{90}Rb [27] is consistent with spin-parity 3⁺. With such spin, the 2128.5-keV transition has a large mixing ratio.

The 5426.66-keV level reported in Ref. [27] does not exist. Instead, the 3534.4-keV decay of this level reported in Ref. [27] as feeding the 1892.3-keV level, depopulates the

TABLE V. Experimental properties of excited levels in ^{92}Sr populated in neutron-induced fission of ^{235}U . New or improved information compared to previous works is marked with asterisks. Spin-parity with superscript “a” is adopted from Ref. [28]. Explanation of other symbols as in Table II.

E_i (keV)	I_i^π	E_γ (keV)	I_γ (rel.)	E_f (keV)	I_f^π
814.90(5)	2^+	814.90(5)		0.0	0^+
1385.3(3)	2^{+a}	570.4(2)		814.90	2^+
		1385.3(2)		0.0	0^+
1673.8(1)	4^+	858.90(5)		814.90	2^+
1778.4(2)	2^{+a}	393.3(2)		1385.3	2^+
		963.4(2)		814.90	2^+
2053.6(3)	$(2^+)^a$	1238.7(2)		814.90	2^+
2088.6(4)	$0^{(+)}$	1273.6(3)		814.90	2^+
2140.8(3)	1^{+a}	755.6(3)		1385.3	2^+
		1326.0(2)		814.90	2^+
2186.2(2) *	$(2^+), 3^- *$	512.5(3)	10(3)*	1673.8	4^+
		1371.3(1) *	100(3)*	814.90	2^+
2526.9(2)	0^+	385.9(4)	20(10)	2140.8	1^+
		1712.1(2)	100(15)	814.90	2^+
2766.7(2)	$(4^+), 5^- *$	580.7(1)	55(5)	2186.2	$(2^+), 3^-$
		1092.90(5)	100(5)	1673.8	4^+
2783.9(2)		1398.7(2)		1385.3	2^+
		1968.8(2)		814.90	2^+
2821.0(3)	$2^{(+)}, (1)^a$	2006.4(2)		814.90	2^+
2925.5(5)		1251.7(4)		1673.8	4^+
3015.5(3)	$5 *$	1341.7(2)		1673.8	4^+
3130.2(3) *	(6^+)	1456.4(2)		1673.8	4^+
3364.2(2) *	(5^-)	597.2(3)	5(2)	2766.7	$(4^+), 5^-$
		1178.1(2)	70(20)	2186.2	$(2^+), 3^-$
		1690.5(2)	100(20)	1673.8	4^+
3559.8(3) *	(6)	793.1(1)		2766.7	$(4^+), 5^-$
3787.4(3) *	$6, (7^-)$	771.8(2)	20(7)	3015.5	5
		1020.8(1)	100(5)	2766.7	$(4^+), 5^-$
4023.7(3) *	(7^-)	236.1(3)	60(20)	3787.4	$6, (7^-)$
		659.6(2)	100(10)	3364.2	(5^-)
4930.0(4)	$(8, 9^-)$	1142.6(2)		3787.4	$6, (7^-)$
5060.1(6) *	$(8, 9^-) *$	1036.4(4)		4023.7	(7^-)
5730.0(5) *	$(10, 11^-) *$	800.0(2)		4930.0	$(8, 9^-)$

4366.1-keV level and feeds the 831.7-keV level whereas the 1892.3-keV level is fed by the 3538.5-keV transition seen in Fig. 2(a). This confirms the 5430.6-keV level, reported in Ref. [27] as uncertain. Angular and directional-polarization correlations for the new 3534.4-831.7-keV cascade indicate spin-parity of 1^+ or 3^+ for the 4366.1-keV level. The log ft of 5.9 for this level, populated in the β^- decay of the 0^- ground state of ^{90}Rb [27] is consistent with spin $I=1$. Therefore, we assign spin-parity 1^+ to the 4366.1-keV level.

B. Excitations in ^{92}Sr

New information on ^{92}Sr was obtained in this paper from the EXILL measurement of prompt- γ rays following fission of ^{235}U . As shown in Table I, the present measurement provided an order of magnitude of more triple- γ events compared to the measurement of ^{248}Cm fission [18]. Apart from

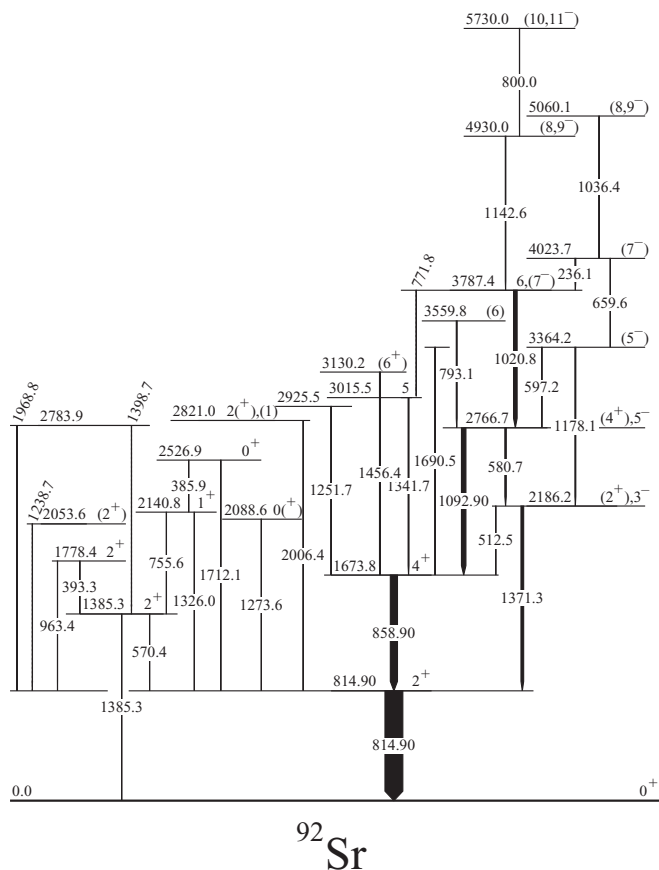


FIG. 4. Partial level scheme of ^{92}Sr obtained in this paper in measurements of γ rays following neutron-induced fission of ^{235}U . Arrow width is proportional to the observed γ intensity.

Ref. [18], medium-spin levels in ^{92}Sr were also reported in Refs. [25,26].

In contrast to ^{90}Sr , the population of excited levels in ^{92}Sr in the β^- decay of ^{92}Rb is low because of the 95% β^- -decay branch to the ground state of ^{92}Sr . Therefore, the present β^- -decay data are not competitive with previous measurements, although we could observe most of the levels reported in the compilation [28].

Excited levels of ^{92}Sr observed in this paper are listed in Table V and shown in Fig. 4. Some of the decays reported in Ref. [28] are not seen in our paper because of high background in fission data. Spins and parities of the 1385.3-, 1778.4-, 2140.8-, and 2821.0-keV levels, shown in Fig. 4 are taken from Ref. [28]. Other spin-parity assignments are based on on angular-correlation and directional-polarization-correlation measurements performed in this paper and listed in Tables VI and VII, respectively.

Our data confirm the 2^+ and 4^+ spin-parity assignments to the 814.90- and 1673.80-keV levels, reported in Refs. [18,28].

Angular correlations for the 1273.6-814.90-keV cascade from the 2088.6-keV level and for the 1712.1-814.90-keV cascade from the 2526.9-keV level are consistent with spin $I=0$ assignment to both levels. Positive parity is adopted after Ref. [28].

TABLE VI. Angular correlation coefficients for γ - γ cascades in ^{92}Sr populated in neutron-induced fission of ^{235}U . The label sum denotes summed correlations with all quadrupole transitions below $E_{\gamma 1}$. Superscript a indicates mixed transition if not γ_1 .

$E_{\gamma 1}$ - $E_{\gamma 2}$ cascade	A_2/A_0 expt.	A_4/A_0 expt.	Spins in cascade	$\delta_{\text{exp}}(E_{\gamma 1})$
580.7-1371.3 ^a	-0.11(6)	0.05(13)	5-3-2 5-3-2	-0.10(17) -2.8(11)
1020.8-580.7	-0.20(9)	-0.27(18)		
858.90-814.90	0.111(12)	-0.020(23)	4-2-0	
1092.90-sum	0.00(3)	0.01(6)	4-4-2 5-4-2 5-4-2	0.54(8) 0.11(4) 5.2(12)
1273.6-814.90	0.91(61)	0.75(13)	0-2-0	
1341.7-sum	-0.13(9)	-0.29(19)	5-4-2	90(-30,+200)
1371.3-814.90	0.179(14)	-0.037(32)	2-2-0 3-2-0 3-2-0	0.15(6) 0.35(5) 1.7(2)
1456.4-sum	0.095(60)	0.04(18)	6-4-2	
1712.1-814.90	0.16(7)	0.80(15)	0-2-0	

In Ref. [18], spin $I=3$ with a tentative negative parity was assigned the 2186.1-keV level. Our correlations allow spin $I=2$ or $I=3$. Spin $I=3$ is more likely considering the observed population of ^{92}Sr in fission and the yrast-population argument [29]. Angular correlations indicate a large mixing ratio for the 1371.3-keV transition, which would suggest its $M1 + E2$ multipolarity. However, the directional-polarization correlations indicate an $E1 + M2$ multipolarity for the 1371.3-keV transition, thus, a negative parity for the 2186.2-keV level.

Angular correlations and directional-polarization correlations for the 1092.90-858.90-keV cascade are consistent with 4^+ or 5^- spin-parity for the 2766.7-keV level. The 4^- hypothesis considered before Ref. [18] can be rejected. The yrast-population argument [29] favors the 5^- solution. This is consistent with the observed population of the yrast cascade in ^{92}Sr in heavy-ion reactions [25,26].

For the 3015.5-, 3130.2-, 3364.2-, and 3559.8-keV levels, we propose spins and parities as shown in Fig. 4 based on

TABLE VII. Experimental $P_{\text{exp}}(\gamma_1)$ and theoretical $P_{\text{th}}(\gamma_1)$ values of linear polarization for the γ_1 (upper) transition in a γ - γ cascade of ^{92}Sr , populated in neutron-induced fission of ^{235}U as obtained in this paper. The correlating γ_2 of 814.90 keV is assumed to be a stretched $E2$ transition with $\delta=0$. Label “p” indicates the transition for which the polarization was determined if not γ_1 .

$E_{\gamma 1}$ - $E_{\gamma 2}$	$P_{\text{exp}}(\gamma_1)$	Spin parity	$\delta_{\text{exp}}(\gamma_1)$	$P_{\text{th}}(\gamma_1)$
858.90-814.90	0.26(11)	$4^+ - 2^+ - 0^+$	0.0	0.1667
858.90-814.90 ^p	0.31(10)	$4^+ - 2^+ - 0^+$	0.0 ^p	0.1667 ^p
1092.90-858.90	0.50(20)	$4^+ - 4^+ - 2^+$ $5^- - 4^+ - 2^+$ $5^- - 4^+ - 2^+$	0.54(8) 0.11(4) 5.2(12)	0.269(2) 0.146(13) 0.293(18)
1371.3-814.90	0.7(3)	$2^+ - 2^+ - 0^+$ $3^- - 2^+ - 0^+$ $3^- - 2^+ - 0^+$	0.15(6) 0.35(5) 1.7(2)	0.452(3) 0.279(26) 0.520(5)

their angular correlations and decay properties and taking into account the yrast-population argument [29].

The 3787.4-keV level was first assigned spin-parity (6^+) [26] and later ($6^-, 7^-$) [18]. The observed intensities of γ transitions together with the yrast-population argument suggest spin $I=7$ for this level. On the other hand, angular correlations for the 1020.8-580.7-keV cascade from this level are not consistent with either $7^- - 5^- - 3^-$ or $6^+ - 4^+ - 2^+$ solution. We put tentative spin-parity 6, (7^-) for the 3787.4-keV level.

Tentative spin-parity assignments to higher-energy states were suggested based on the observed decays and the yrast-population argument.

As a final comment, we note that the high admixture of the $M2$ multipolarity in the 1092.90- and 1371.3-keV transitions is an intriguing observation. An alternative, positive-parity assignment to 2186.1- and 2766.7-keV levels would change significantly the systematic picture of octupole collectivity in the region. The spin-parity of the 3787.4-keV level needs a clarification to decide if there is only a negative-parity band at medium spins [18] or a positive-parity band as suggested in Ref. [26]. More precise multipolarity measurements for transitions in ^{92}Sr are needed, for example, a high-statistics measurement of γ rays following neutron-induced fission of ^{233}U .

C. Excitations in ^{94}Sr

The previous study of ^{94}Sr [18] was focused on negative-parity medium-spin levels aimed at identifying the ($h_{11/2}, g_{7/2}$)₉- two-neutron configuration involving the important $h_{11/2}$ neutron level. This level, crucial for the development of nuclear deformation in the region [30–34], has not been observed directly to date [35]. In the present paper, in addition to confirming the negative-parity assignments proposed in Ref. [35], which replaced earlier positive-parity assignments [36], we have searched for new medium-spin, positive-parity states, a possible signature of a quadrupole collectivity developing in the chain of strontium isotopes [37].

Positive-parity low-spin levels of ^{94}Sr were reported in a measurement of γ rays from the β decay of ^{94}Rb [38], but some of them with incorrect parity assignments as shown in the compilation [39]. Because of the $I^\pi=3^-$ spin-parity of the ground state of ^{94}Rb [40], 0^+ levels were not seen in Ref. [38]. A recent neutron-transfer-reaction study [41] reported two low-lying 0^+ levels in ^{94}Sr .

Excited states in ^{94}Sr observed in this paper are listed in Table VIII and shown in Fig. 5. Spin-parity assignments in Fig. 5 and Table VIII are based on the angular and directional-polarization correlations measured in this paper and listed in Tables IX and X. All transitions shown in Table VIII correspond to prompt- γ radiation following fission except the 1577.55-keV decay of the 2414.5-keV level, which is predominantly populated in the β decay of ^{94}Rb . Many levels reported in Ref. [38] are seen in our data but not on a competitive level and except the strongly populated 2414.5-keV level, they were not analyzed in this paper. However, to assist further discussions we show in Fig. 5 several low-spin levels, drawn after Refs. [39,41]. They are shown without decays on the right-hand side of the figure. In our data we could not see the 1043.5- and 1456.1-keV decays of the newly proposed 0^+ levels at 1879.7 and 2292.8 keV [41]. The important new results are discussed below.

The ground-state cascade, shown to the left of Fig. 5 has been extended up to spin (8^+). Angular and directional-polarization correlations uniquely determine spin-parity assignments up to spin 6^+ . Spins and parities of higher-energy levels are proposed based on the observed decay branching and the yrast argument [29].

The 3^+ spin-parity of the 2414.50-keV level was reported in Ref. [41] based on the distorted wave Born approximation analysis favoring positive parity, although still consistent with the negative parity, tentatively proposed in the past [38,39]. Our search for the low-energy 3^+ level in ^{94}Sr was prompted by the shell-model results reported in Ref. [18] where the experimental data were insufficient for its identification. The present results determine uniquely the 3^+ spin-parity of the 2414.50-keV level. We note a good match of the mixing ratio δ obtained in this paper with that reported in Ref. [39]. The χ^2/N analysis of the combined angular correlations and linear polarization for the 1577.55-836.95-keV cascade is illustrated in Fig. 6 where we show χ^2/N solutions for various spin-parity hypotheses of the 2414.50-keV level (more information about this technique can be found in Sec. 4 of Ref. [23]).

The multipolarity analysis for the 710.90-(1309.05 + 836.95)-keV cascade indicates spin-parity 5^+ for the 2856.9-keV level, reported as (5^-) in the compilation [39]. The negative parity reported in Ref. [18] was a result of underestimating the 709.4-keV component admixture in the 711-keV complex line. The present high-statistics data allowed a better fit to the doublet. The positive parity of the 2856.9-keV level is supported by the multipolarity analysis for the 253.00-677.70-keV cascade, indicating a pure stretched E1 multipolarity of the 253.00-keV decay to the 4^- level at 2604.1 keV (see below). Tentative spin-parity of 4034.6- and 4952.9-keV levels are based on decay branching and the yrast-population argument [29].

TABLE VIII. Experimental properties of excited levels in ^{94}Sr populated in neutron-induced fission of ^{235}U (except the 2414.50-keV level—see the text). New information is marked by asterisks. Explanation of other symbols as in Table II.

E_i (keV)	I_i^π	E_γ (keV)	I_γ (rel.)	E_f (keV)	I_f^π
836.95(5)	2^+	836.95(5)		0.0	0^+
1926.40(8)	3^-	1089.45(5)		836.95	2^+
2146.00(8)	4^+	1309.05(5)		836.95	2^+
2414.50(8)	$3^+ *$	1577.55(5)		836.95	2^+
2604.1(1)	$4^- *$	189.5(2) *	1.2(4)	2414.50	3^+
		458.2(1)	24(2)	2146.00	4^+
		677.70(5)	100(3)	1926.40	3^-
		1766.7(3)	1.4(5)	836.95	2^+
2649.8(1)	$4^+ *$	235.5(3) *	2(1)	2414.50	3^+
		503.9(1)	100(3)	2146.00	4^+
		723.3(2)	30(5)	1926.40	3^-
		1812.7(1)	85(5)	836.95	2^+
2739.4(2)	$4^{(-) *} $	813.0(1)	100(5)	1926.40	3^-
		1902.3(2)	6(1)	836.95	2^+
2856.9(1)	$5^+ *$	117.4(1)	27(2)	2739.4	$4^{(-) *} $
		207.20(5)	28(2)	2649.8	4^+
		253.00(5)	100(3)	2604.1	4^-
		710.90(5)	88(3)	2146.00	4^+
2972.0(1)	$5^- *$	826.00(5)	100(8)	2146.00	4^+
		1045.60(5)	82(6)	1926.40	3^-
3155.9(1)	6^+	184.1(1)	25(2)	2972.0	5^-
		299.00(5)	66(3)	2856.9	5^+
		1009.90(5)	100(3)	2146.00	4^+
3310.6(1)	$5^- *$	661.0(2)	75(5)	2649.8	4^+
		1384.3(1)	100(5)	1926.40	3^-
3705.8(2)	$6^{(+)}$	849.0(3)	15(5)	2856.9	5^+
		1559.8(1)	100(3)	2146.00	4^+
3793.2(1)	$6^- *$	482.6(1)	55(5)	3310.6	5^-
		637.3(1)	65(5)	3155.9	6^+
		1189.1(1)	100(3)	2604.1	4^-
3923.3(1)	$7^- *$	130.20(5)	35(2)	3793.2	6^-
		217.4(2)	2(1)	3705.8	$6^{(+)}$
		612.8(2)	7(1)	3310.6	5^-
		767.35(5)	100(3)	3155.9	6^+
		951.15(5)	26(2)	2972.0	5^-
		1066.5(3)	9(2)	2856.9	5^+
3952.2(3) *	(6^+)	1806.2(2) *		2146.00	4^+
4034.6(2)	(7^+) *	878.6(1)	100(8)	3155.9	6^+
		1177.9(3)	45(5)	2856.9	5^+
4360.3(3) *	(8^+) *	1204.4(2) *		3155.9	6^+
4383.2(2)	(8^-)	459.70(5)		3923.3	7^-
4435.5(3) *	(7^+)	483.3(2) *		3952.2	(6^+)
4632.9(2)	(8^-)	249.8(2)	25(2)	4383.2	(8^-)
		598.20(5)	40(5)	4034.6	(7^+)
		709.4(1)	100(3)	3923.3	7^-
4858.9(2)	(9^-)	226.1(1)	100(5)	4632.9	(8^-)
		475.6(1)	85(5)	4383.2	(8^-)
		935.3(1)	30(5)	3923.3	7^-
4892.5(4) *	(8^+)	457.0(2) *		4435.5	(7^+)
4952.9(3) *	(8^+)	1000.8(2) *	100(15)	3952.2	(6^+)
		1247.1(1) *	30(10)	3705.8	$6^{(+)}$
5741.3(3)	$(10,11^-)$	882.4(1)		4858.9	(9^-)
5815.0(3) *	$(9,10^+)$	862.1(2) *		4952.9	(8^+)
		922.6(3) *		4892.5	(8^+)
6920.7(4) *	$(12,13^-)$	1179.4(2) *		5741.3	$(10,11^-)$
7262.4(5) *	$(14,15^-)$	341.7(2) *		6920.7	$(12,13^-)$

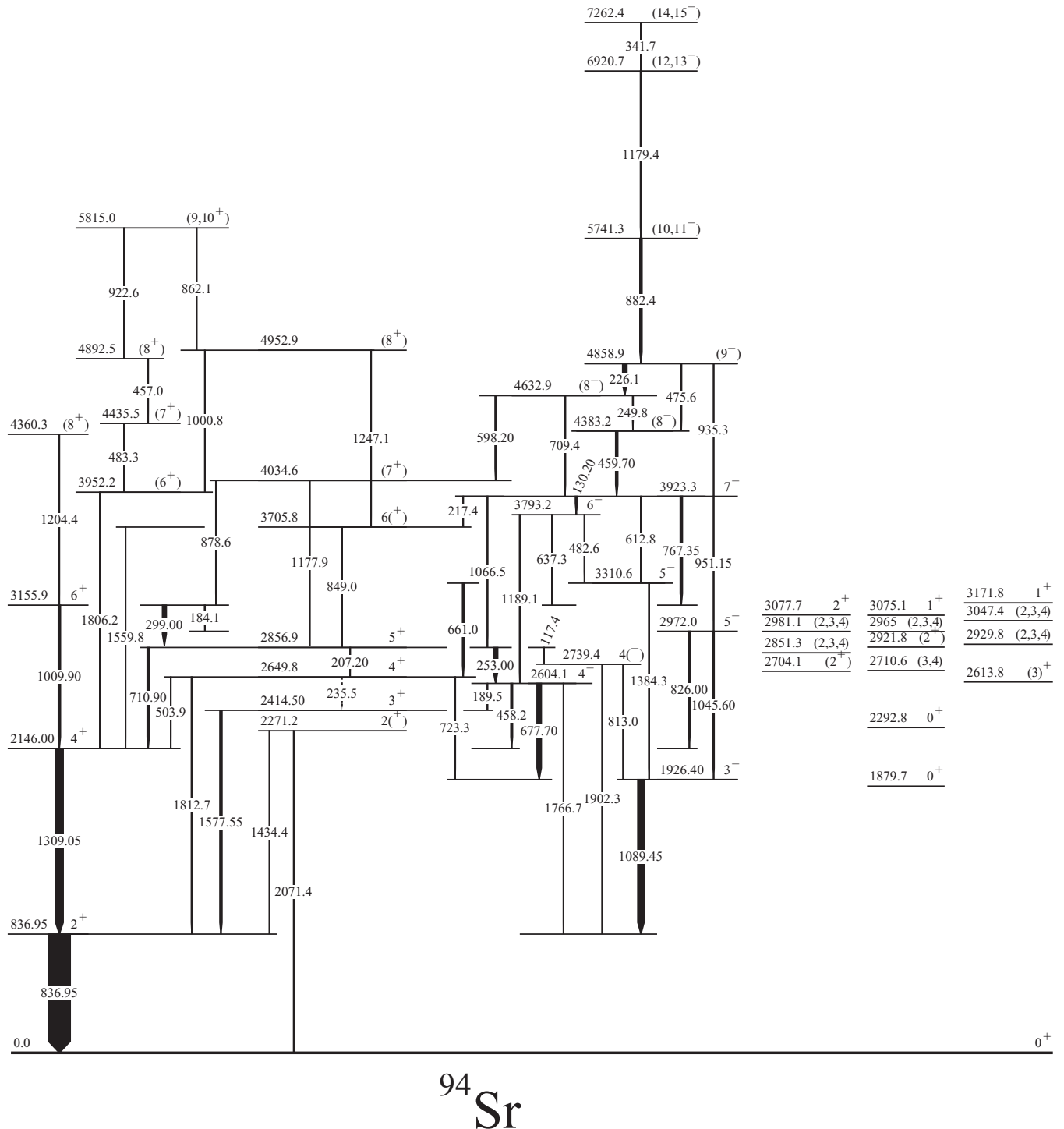


FIG. 5. Partial level scheme of ^{94}Sr obtained in this paper in a measurement of γ rays following neutron-induced fission of ^{235}U . Levels without decays, shown to the right, and the 2271.2-keV level are drawn after Refs. [39,41] to assist further discussions.

Levels at 2414.50, 2649.8, 2856.9, 3705.8, 4034.6, and 4952.9 keV, shown in the middle of Fig. 5 can be arranged into a band because of linking transitions. Here we included also the 2271.2-keV level populated in the β decay [38] with a tentative (2^+) spin-parity [39]. Spin $I=2$ is supported by the fact that, unlike the nearby 3^+ at 2414.50 keV, the 2271.2-keV level is not populated directly in fission.

The new structure above the 2271.2-keV level is a candidate for a γ band in ^{94}Sr with a possible 2_2^+ head at 2271.2 keV. The link to the head is not observed most likely because of the unfavored branching from the 2414.50- and 2649.8-keV levels. However, the missing E2 link between the 2856.9- and the 2414.50-keV levels and the high intensity of the 253.00-keV E1 decays from the 2856.9-keV level are

TABLE IX. Angular correlation coefficients for γ - γ cascades in ^{94}Sr populated in neutron-induced fission of ^{235}U . The label sum denotes summed correlations with all quadrupole transitions below the $E_{\gamma 1}$.

$E_{\gamma 1}$ - $E_{\gamma 2}$ cascade	A_2/A_0 expt.	A_4/A_0 expt.	Spins in cascade	$\delta_{\text{exp}}(E_{\gamma 1})$
253.00-677.70	0.127(10)	-0.010(23)	5-4-3	0.02(1)
1089.45-836.95	-0.068(10)	-0.020(22)	3-2-0	0.005(12)
1309.05-836.95	0.104(8)	-0.022(18)	4-2-0	
1577.55-836.95	-0.070(9)	-0.018(18)	3-2-0	0.002(12)
1812.65-836.95	0.093(26)	0.020(60)	4-2-0	
503.9-sum	0.190(23)	0.030(56)	4-4-2	0.02(8) or -0.97(15)
1009.90-sum	0.111(12)	-0.021(27)	6-4-2	
767.35-1009.90	-0.083(15)	0.005(34)	7-6-4	-0.017(24)
677.70-1089.45	0.313(10)	0.004(24)	4-3-2	-1.5(3) or -0.9(2)
813.0-1089.45	0.041(20)	-0.041(43)	4-3-2	0.02(4) or 7.7(19)
1384.3-1089.45	-0.049(37)	0.11(8)	5-3-2	
710.90-1309.05	-0.224(13)	-0.013(26)	5-4-2	-0.23(3) or -6.8(9)
826.00-1309.05	-0.065(23)	-0.011(47)	5-4-2	0.01(4)

puzzling. In Ref. [41], a single-particle character of the 3^+ level at 2414.50-keV was considered.

Above the 1926.40-keV level one observes a cascade consisting of negative-parity level. The 3^- spin-parity of the 1926.40-keV level is uniquely determined by multipolarity analysis for the 1089.45-836.95-keV cascade. The analysis for the 677.70-1089.45-keV cascade uniquely determines spin-parity 4^- of the 2604.1-keV level. This agrees with the stretched E1 feeding from the 5^+ level at 2856.9 keV. The multipolarity analysis for the 826.0-1309.05-keV cascade indicates spin-parity 5^- for the 2972.0-keV level, and the analysis for the 767.35-1009.90-keV cascades indicates spin-parity 7^- for the 3923.3-keV level. Spin-parity assignments to levels at higher energies are proposed based on the observed decay branching and the yrast-population argument [29].

TABLE X. Experimental $P_{\text{exp}}(\gamma_1)$ and theoretical $P_{\text{th}}(\gamma_1)$ values of linear polarization for the γ_1 (upper) transition in a γ - γ cascade of ^{94}Sr , populated in neutron-induced fission of ^{235}U as obtained in this paper. The correlating γ_2 transitions of 836.95 and 1309.05 keV are assumed to be stretched E2 with $\delta=0$.

$E_{\gamma 1}$ - $E_{\gamma 2}$	$P_{\text{exp}}(\gamma_1)$	Spin parity	$\delta_{\text{exp}}(\gamma_1)$	$P_{\text{th}}(\gamma_1)$
1089.45-836.95	0.08(3)	3^- - 2^+ - 0^+	0.005(12)	0.106(5)
1309.05-836.95	0.175(45)	4^+ - 2^+ - 0^+	0.0	0.1667
1577.55-836.95	-0.26(9)	3^+ - 2^+ - 0^+	0.002(16)	-0.104(7)
1812.7-836.95	0.57(24)	4^+ - 2^+ - 0^+	0.0	0.1667
503.9-1309.05	-0.01(9)	4^+ - 4^+ - 2^+	0.02(7)	0.329(0)
			-0.97(15)	0.035(20)
710.90-1309.05	-0.34(8)	5^+ - 4^+ - 2^+	-0.23(3)	-0.035(7)
			-6.8(9)	-0.162(8)
1009.90-1309.05	0.11(6)	6^+ - 4^+ - 2^+	-0.23(3)	0.1667

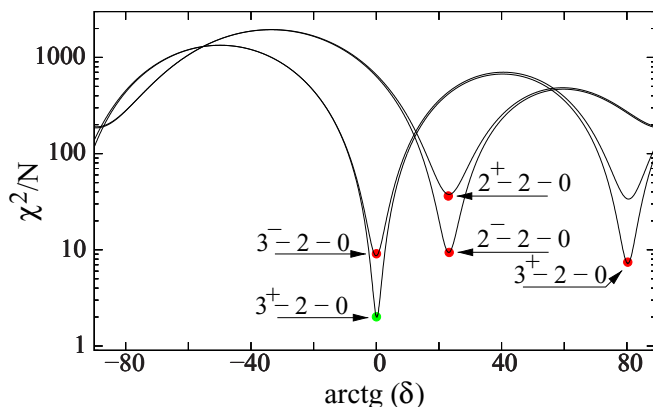


FIG. 6. The combined angular and directional-polarization correlation analysis of transition multiplicities in the 1577.55-836.95-keV cascade in ^{94}Sr , populated in the neutron-induced fission of ^{235}U . See the text for more explanations.

A clear population in fission of ^{235}U of the 2613.8- and 2710.6-keV levels and its lack for the 2704.1-keV level suggests spin of the 2613.8- and 2710.6-keV levels higher than the spin of the 2704.1-keV level. Taking into account the data reported in Refs. [39,41], we, thus, propose spin $I=(3)^+$ for the 2613.8-keV level, spin $I=(3,4)$ for the 2710.6-keV level, and spin $I=(2^+)$ for the 2704.1-keV level.

D. Excitations in ^{96}Sr

Low-spin excitations of ^{96}Sr were studied before in a measurement of γ rays from β decay of the 2^+ ground state of ^{96}Rb [42], in Coulomb excitations [43,44], in transfer reactions [45,46], and in timing measurements of levels populated in neutron-induced fission of ^{235}U [37]. Medium-spin levels of ^{96}Sr were reported before in a measurement of γ rays following spontaneous fission of ^{248}Cm [18,33,47-49] and in α -induced fusion-fission of ^{238}U [50]. The present study of ^{96}Sr , based on a neutron-induced fission of ^{235}U and spontaneous fission of ^{252}Cf , updates and extends previous data.

Excited levels in ^{96}Sr observed in this paper are listed in Table XI and shown in Fig. 7. All transitions shown in Table XI, except the 649.0-keV decay from the 0_3^+ level at 1464.0 keV, are observed as prompt- γ rays following fission. To assist further discussions, we show to the right-hand side of Fig. 7 several low-spin levels, drawn after Refs. [46,51]. These levels are populated predominantly in the β^- decay of ^{96}Rb and are not part of any medium-spin cascades. However, some of them are weakly populated in prompt- γ fission, the observation which will help verifying their spin assignments. Spin-parity assignments to levels in ^{96}Sr shown in Table XI and Fig. 7 are based on angular and directional-polarization correlations measured in this paper and listed in Tables XII and XIII, respectively. New results obtained in this paper are marked with asterisks in Table XI.

The most important new result in ^{96}Sr is the observation of the 277.7-keV E2 in-band decay of the 2^+ level at 1507.0 keV to the 0^+ level at 1229.5 keV, completing the deformed band based on the second 0^+ level in ^{96}Sr . The observed

TABLE XI. Experimental properties of excited levels in ^{96}Sr populated in neutron-induced fission of ^{235}U (except for the 1464.0-keV level—see the text). New information is marked by asterisks. Explanation of other symbols as in Table II.

E_i (keV)	I_i^π	E_γ (keV)	I_γ (rel.)	E_f (keV)	I_f^π
815.00(5)	2 ⁺	815.00(5)		0.0	0 ⁺
1229.5(2)	0 ⁺	414.5(1)		815.00	2 ⁺
1464.0(5)	0 ⁺	649.0(5)		815.00	2 ⁺
1507.0(1)	2 ⁺	277.7(2) *	2.8(5) *	1229.5	0 ⁺
		692.00(5)	100(3)	815.00	2 ⁺
		1506.95(5)	53(2)	0.0	0 ⁺
1628.6(1)	2 ⁺ *	399.0(2)	15(3)	1229.5	0 ⁺
		813.6(1)	100(8)	815.00	2 ⁺
		1628.9(3)	5(3)	0.0	0 ⁺
1792.80(8)	4 ⁺	977.80(5)		815.00	2 ⁺
1852.6(2)	3 ⁻ *	345.5(5)	70(30)	1507.0	2 ⁺
		1037.6(1)	100(20)	815.00	2 ⁺
1975.9(1)	4 ⁺ *	347.3(1)	18(1)	1628.6	2 ⁺
		468.9(1)	100(3)	1507.0	2 ⁺
		1160.8(1)	54(2)	815.00	2 ⁺
2120.1(1)	4 ⁺ *	327.3(1)	11(3)	1792.80	4 ⁺
		1305.10(5)	100(5)	815.00	2 ⁺
2466.8(1)	6 ⁺ *	491.00(5)	82(3)	1975.9	4 ⁺
		674.00(5)	100(3)	1792.8	4 ⁺
2481.0(2)	(5 ⁺) *	361.0(1)	97(14)	2120.1	4 ⁺
		688.1(1)	100(12)	1792.80	4 ⁺
2493.0(3)	(0 ⁺)	1678.0(2)		815.00	2 ⁺
2733.6(2) *	5 ⁻ *	881.2(2) *	30(15)	1852.6	3 ⁻
		940.7(1)	100(20)	1792.80	4 ⁺
2786.0(1)	6 ⁺ *	810.3(1)	50(3)	1975.9	4 ⁺
		993.20(5)	100(3)	1792.80	4 ⁺
2899.8(2)	(6 ⁺) *	779.6(1)	100(20)	2120.1	4 ⁺
		1107.0(1)	66(12)	1792.80	4 ⁺
3010.6(3)	(5)	1217.8(2)		1792.80	4 ⁺
3126.1(2)	8 ⁺ *	659.30(5)		2466.8	6 ⁺
3239.3(3)	(7 ⁺) *	339.6(2)	30(10)	2899.8	(6 ⁺)
		758.3(1)	100(20)	2481.0	(5 ⁺)
3328.9(2)	7 ⁻	542.90(5)	100(6)	2786.0	6 ⁺
		595.5(2)	20(4)	2733.6	5 ⁻
		862.1(1)	19(5)	2466.8	6 ⁺
3524.7(3)	9 ⁻	195.6(1)	21(4)	3328.9	7 ⁻
		398.55(5)	100(5)	3126.1	8 ⁺
3605.4(2)	(6 ⁺)	594.6(3)	43(15)	3010.6	(5)
		1138.7(1)	100(12)	2466.8	6 ⁺
		1812.4(2)	52(14)	1792.80	4 ⁺
3708.5(3) *	(8 ⁺)	922.5(2) *		2786.0	6 ⁺
3852.5(3)	(7 ⁺)	247.1(1)		3605.4	(6 ⁺)
3887.3(3)	(10 ⁺)	761.2(1)		3126.1	8 ⁺
4132.2(4)	(8 ⁺)	279.7(1)		3852.5	(7 ⁺)
4133.4(3)	(8,9 ⁻)	804.5(1)		3328.9	7 ⁻
4331.1(4)	(10,11 ⁻)	806.4(1)		3524.7	9 ⁻
4444.2(5)	(9 ⁺)	312.0(1)		4132.2	(8 ⁺)
4725.6(4)	(12 ⁺)	838.3(1)		3887.3	(10 ⁺)
4787.0(5)	(10 ⁺)	342.8(2)		4444.2	(9 ⁺)
5161.0(7) *	(11 ⁺)	374.0(5) *		4787.0	(10 ⁺)
5390.2(5) *	(11,12)	1059.1(2) *		4331.1	(10,11 ⁻)
5752.5(6) *	(12,13 ⁻)	1421.4(1) *		4331.1	(10,11 ⁻)
6007.8(6) *	(13,14)	255.3(2) *		5752.5	(12,13 ⁻)
		618.1(3) *		5390.2	(11,12)
6213.8(7) *	(14,15)	206.0(2) *		6007.8	(13,14)

TABLE XII. Angular correlation coefficients for γ - γ cascades in ^{96}Sr populated in neutron-induced fission of ^{235}U . The label sum denotes summed correlations with all quadrupole transitions below the $E_{\gamma 1}$. Superscript “a” indicates mixed transition if not γ_1 .

$E_{\gamma 1}$ - $E_{\gamma 2}$ cascade	A_2/A_0 expt.	A_4/A_0 expt.	Spins in cascade	$\delta_{\text{exp}}(E_{\gamma 1})$
398.55-sum	-0.125(10)	-0.008(22)	9-8-6	-0.09(2)
414.5-815.00	0.33(9)	0.67(18)	0-2-0	
468.9-692.00 ^a	0.128(17)	-0.060(37)	4-2-2	0.77(15) or 3.4(11)
491.0-468.9	0.096(14)	0.003(31)	6-4-2	
542.90-sum	-0.062(25)	-0.048(45)	7-6-4	0.02(4)
649.0-815.00	0.36(15)	0.80(32)	0-2-0	
659.30-674.00	0.113(15)	-0.003(33)	8-6-4	
659.30-491.00	0.098(14)	-0.049(29)	8-6-4	
674.00-sum	0.097(10)	-0.018(21)	6-4-2	
692.00-815.00	-0.246(17)	0.173(34)	2-2-0	0.87(7)
813.6-815.00	-0.015(18)	0.058(39)	2-2-0	0.35(3)
993.20-sum	0.117(19)	-0.019(43)	6-4-2	
1037.6-815.00	-0.036(28)	0.048(55)	3-2-0	0.05(4)
1160.8-815.00	0.095(21)	-0.022(44)	4-2-0	
1305.10-815.00	0.105(25)	-0.068(54)	4-2-0	

Spin-parity assignments to the 815.00- and 1792.80-keV levels are adopted after the compilation [51]. Unique spin-parity assignments to the 2466.8-, 3126.1-, and 3524.7-keV levels are determined based on the angular and directional-polarization correlations listed in Tables XII and XIII, confirming assignments reported in our previous works [18,33]. Analogously, unique spin-parity assignments are determined for the 1507.0-, 1628.6- and 1975.9-keV levels confirming assignments reported in Refs. [33,51].

The multipolarity analysis for the 993.2-977.80-keV cascade indicates spin-parity 6⁺ for the 2786.0-keV level. Subsequent analysis for the 542.90-sum cascade (see Table XII) indicates spin I=7 for the 3328.9-keV level. The $I^\pi=9^-$ spin-parity of the 3524.7-keV isomer imposes the stretched E2 character on its 195.6-keV decay, indicating a negative parity for the 3328.9-keV level.

TABLE XIII. Measured $P_{\text{exp}}(\gamma_1)$ and calculated $P_{\text{th}}(\gamma_1)$ values of linear polarization for the γ_1 transition in a γ - γ cascade of ^{96}Sr as obtained in this paper. The correlating γ_2 of 815.00 keV is assumed to be a stretched E2 transition with $\delta=0$. The label sum denotes summed correlations with all quadrupole transitions below $E_{\gamma 1}$.

$E_{\gamma 1}$ - $E_{\gamma 2}$	$P_{\text{exp}}(\gamma_1)$	Spin parity	$\delta_{\text{exp}}(\gamma_1)$	$P_{\text{th}}(\gamma_1)$
398.55-sum	0.11(6)	9 ⁻ -8 ⁺ -6 ⁺	-0.09(2)	0.075(7)
414.5-815.00	1.2(5)	0 ⁺ -2 ⁺ -0 ⁺	0.0	1.0000
659.30-sum	0.19(6)	8 ⁺ -6 ⁺ -4 ⁺	0.0	0.1667
674.00-sum	0.22(7)	6 ⁺ -4 ⁺ -2 ⁺	0.0	0.1667
977.80-815.00	0.16(4)	4 ⁺ -2 ⁺ -0 ⁺	0.0	0.1667
993.2-977.80	0.45(38)	6 ⁺ -4 ⁺ -2 ⁺	0.0	0.1667
1160.8-815.00	0.16(8)	4 ⁺ -2 ⁺ -0 ⁺	0.0	0.1667
1305.10-815.00	0.40(28)	4 ⁺ -2 ⁺ -0 ⁺	0.0	0.1667

The analysis for the 1037.6-815.00-keV cascade shows that the 1037.6-keV transition is not a stretched quadrupole and puts the $I < 4$ limit on the spin of the 1852.6-keV level. On the other hand, the prompt 595.5-881.2-keV cascade from the 3328.9-keV level gives $I > 2$. The resulting spin $I=3$ of the 1852.6-keV level indicates spin $I=5$ for the 2733.6-keV level and a negative parity for both levels.

The analysis for the 1305.10-815.00-keV cascade indicates spin-parity $I^\pi=4^+$ for the 2120.1-keV level.

Spins and parities of other levels in cascades are proposed based on the yrast-population argument [29] and decay branching. In particular, a tentative $I=6(+)$ spin-parity for the 3605.4-keV level is suggested by the 1812.4-keV decay to the 4^+ level at 1792.80 keV and the yrast-population argument applied to the 3605.4-keV level.

A clear population in fission of ^{235}U of 2150.8 keV suggests spin higher than $I=1$ for this level. Taking into account the data reported in Refs. [46,51], we, thus, propose spin $I=(2,3^+)$ for the 2150.8-keV level. The levels at 2493.0 and 2704.0 keV are possible candidates for 0^+ excitations in ^{96}Sr . This is supported by angular correlations for the 1678.0-815.00- and 1889.0-815.00-keV cascades showing large A_4/A_0 values and the lack of population on these levels in fission of ^{235}U .

III. DISCUSSION

For the evolution of nuclear deformation in the $A \approx 100$ region, the crucial issue is the “early” population of the neutron $g_{7/2}$ and the proton $g_{9/2}$ shells. The population of the proton $g_{9/2}$ orbital seem to be particularly sudden, giving rise to a strong deformation already at $Z=38$. Various explanations were proposed in the past. Federman and Pittel [52] proposed the population of $g_{9/2}$ protons via the monopole interaction with the $gg_{7/2}$ neutrons—the spin-orbit-partner (SOP) mechanism. However, this does not explain the early population of the $g_{7/2}$ neutrons. More recently an analogous “self-reinforcing” [53] mechanism was proposed, driven by the monopole tensor interaction between the two orbitals [54], but again, the early population of the $g_{7/2}$ neutrons was not addressed.

We note, that in the Nilsson scheme, there are strongly upsloping $3/2^-$ [301], $5/2^-$ [303], and $1/2^-$ [301] proton orbitals, crossing the down-sloping, $1/2^+$ [440], $3/2^+$ [431], and $5/2^+$ [422] orbitals of the $g_{9/2}$ parentage. With the increasing deformation, the upsloping orbitals deliver six extra protons to the Fermi level, which populate the $g_{9/2}$ shell helping to create deformed minimum in the nuclear potential. This action may begin already in Se isotopes at $Z=34$ (see, e.g., Fig. 8 in Ref. [55]). Indeed, in Br isotopes, the $g_{9/2}$ proton excitation is observed at about 1.5 MeV [17,56], an energy lower than expected from the scheme of spherical shells.

Less evident is the early population of the neutron $g_{7/2}$ shell and its role in the shape coexistence in the region. As noted in Ref. [57], this orbital is populated already at $N = 52$. A pair of neutrons can be promoted across the $N = 50$ gap from the $g_{9/2}$ to the $g_{7/2}$ shell creating 0^+ excited levels at relatively low excitation, analogous to 0^+ intruder states in Sn isotopes created by promoting a pair of protons across the $Z=50$ line

[58]. The SOP mechanism and the action of the $9/2^+$ [404] extruder [59,60], which promotes two extra neutrons to the Fermi surface (see, e.g., Fig. 9 in Ref. [55]) further increases the population of the $g_{7/2}$ shell, resulting in lowering such 0^+ energies with the growing neutron number.

Below we discuss these ideas in more detail, assisted by the LSSM calculations performed using the natural valence space outside the ^{78}Ni core, comprising the $\pi 1f_{5/2}$, $2p_{3/2}$, $2p_{1/2}$, $1g_{9/2}$, and $\nu 2d_{5/2}$, $3s_{1/2}$, $2d_{3/2}$, $1g_{7/2}$, and $1h_{11/2}$ orbitals. The model space and interaction were previously employed in the studies of a large number of nuclei in the region, see, e.g., Refs. [16,18,56,57,61–64]. In particular, it has proven successful in the description of the zirconium isotopic chain below $N = 60$ [61]. It, thus, seems particularly suited for investigating the structure of low-energy excitations in Sr isotopes. As can be anticipated from this previous study [61], the strongly deformed collective states at low energy may not be fully accounted for in the present model. However, we do not expect such states to appear at $N < 58$. The calculations were performed using the Strasbourg shell-model codes ANTOINE and NATHAN. The Sr isotopes with $N \geq 56$ pose a challenge to standard diagonalization techniques within this model space. We performed unrestricted calculations for $N = 50 - 54$ whereas 8p-8h excitations were allowed in $^{94}\text{Sr}_{56}$ and in $^{96}\text{Sr}_{58}$. Only a few lowest levels were computed in ^{96}Sr due to the numerical complexity. The details of these calculations and an extended discussion of the theoretical results will be presented in Ref. [65].

A. General properties of Sr isotopes

Excitation schemes of $^{90-96}\text{Sr}$, shown in Figs. 3–5 and 7 show an increase in collectivity with the growing neutron number, which is reflected in the decreasing excitation energies of low-spin levels.

The ^{90}Sr nucleus displays features characteristic of a spherical system with the $R_{42} = E_{\text{exc}}(4_1^+)/E_{\text{exc}}(2_1^+)$ ratio of 1.99. Except the ground-state cascade no other structure is formed below 4 MeV. Two cascades, of probable s.p. nature are populated above this energy in heavy-ion-induced reaction [26].

In ^{92}Sr , the $R_{42}=2.05$ ratio is similar, but there is a significant lowering of nonyrast excitations. The only band is observed on top of the 3^- octupole excitation, in accord with observations from other regions that octupole collectivity develops early outside closed shells.

In the ^{94}Sr nucleus, the $R_{42} = 2.56$ ratio suggests its transitional character. This is supported by lower energies of negative-parity levels and the appearance of a γ -like band, another collectivity showing early outside closed shells.

Finally, in ^{96}Sr , a well-developed rotational band, based on the 0_2^+ level is seen. This bands has the ratio $R_{42}=2.69$ whereas the $R_{42}=2.20$ ratio in the ground-state cascade is lower than in ^{94}Sr . We also note that the negative-parity band here is developed less than in ^{94}Sr .

Summarizing, up to $N = 58$, the collectivity in Sr isotopes increases slowly with the growing neutron number. This increase is seen in excited configurations whereas ground states

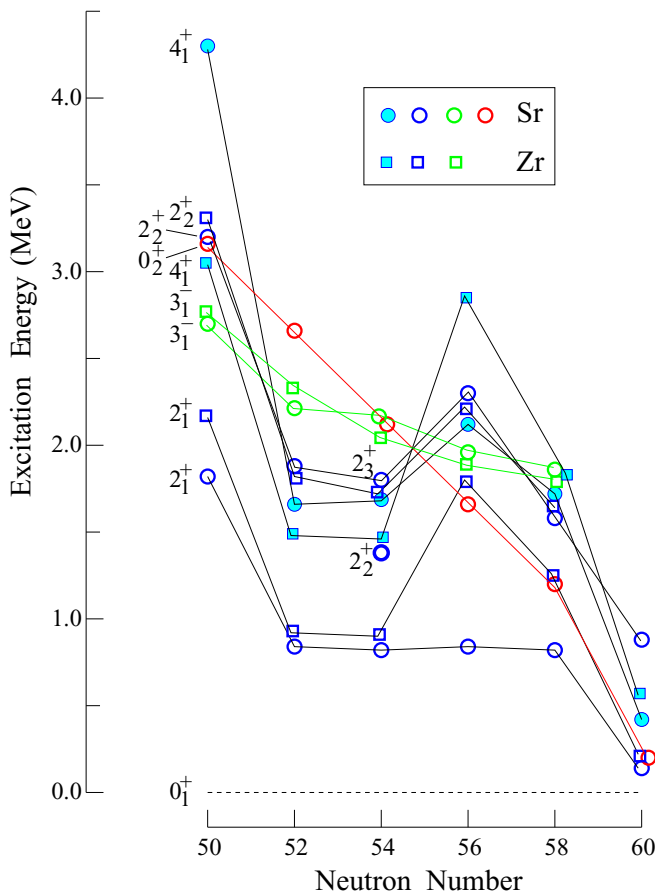


FIG. 8. Excitation energies of low-spin levels in Sr and Zr isotopes. The data are taken from the present paper and from the ENSDF base [4]. See the text for more comments.

remains spherical as can be judged from their quadrupole moments [66].

Figure 8 shows low-energy 0_2^+ (red circles), 2^+ (blue open symbols), 3^- (green symbols), and 4^+ (blue filled symbols) excitation energies in Sr (circles) and Zr (squares) isotopes. Above $N = 50$, excitation energies drop quickly with the increasing neutron number, but at $N = 56$, all positive-parity levels increase significantly in energy due to the $d_{5/2}$ neutron shell closure. The 2_1^+ level with nearly constant energy from $N = 52$ to $N = 58$ is a notable exception, which will be discussed below. One also notes a deviation of the 2_2^+ level in ^{94}Sr from the general trend with the energy of the 2_3^+ level closer to the expected position of the 2_2^+ level. Above $N = 58$, there is a spectacular lowering of all the levels. This suggests another mechanism of excitation there as discussed in Ref. [1]. In contrast, negative-parity levels, which are probably due to octupole correlations, do not show such strong variations and, to date, are not known above $N = 58$.

In the following sections, we discuss various excitation modes, which may contribute to the development of collectivity seen in Fig. 8. Special attention will be devoted to 0^+ excitations, which play an important role in quantum phase transitions and shape coexistence phenomena in the region [67,68]. The experimental results are compared to the LSSM

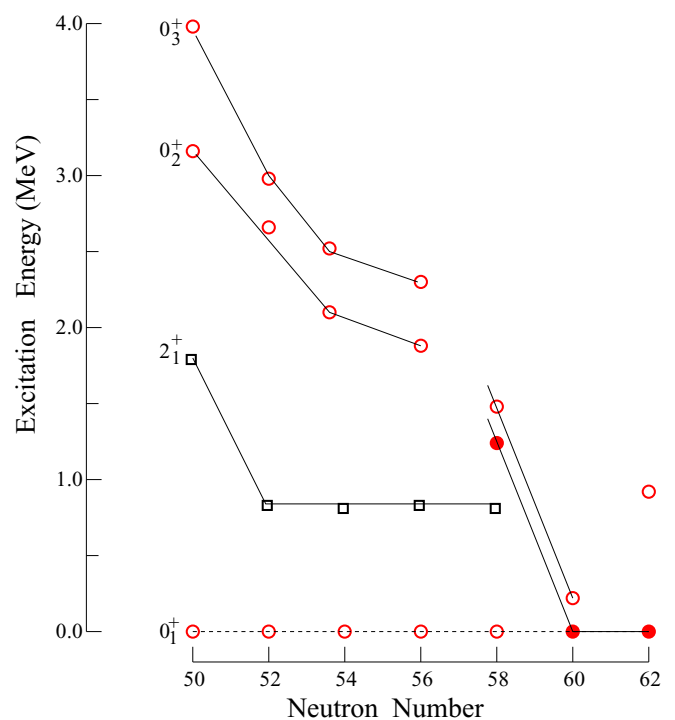


FIG. 9. Excitation energies of 0_2^+ and 0_3^+ levels in Sr isotopes. The data are taken from the present paper and from the ENSDF base [4]. Lines are drawn to guide the eye. See the text for more comments.

calculations to learn more about the microscopic structure of Sr isotopes.

B. 0^+ excitations

Figure 9 shows excitation energies of 0_2^+ and 0_3^+ levels in Sr isotopes in the neutron range $50 \geq N \geq 62$. Data points corresponding to deformed 0^+ levels are represented by filled circles. To help the discussion, we included energies of 2_1^+ excitations (empty square symbols).

Energies of 0_2^+ levels decrease from $N = 50$ to $N = 58$ and then drop suddenly at $N = 60$. The 0_3^+ levels follow closely the trend of 0_2^+ levels. This suggests that the 0_3^+ levels interact weakly with 0_2^+ levels not showing any clear “repulsion pattern,” thus, not supporting the strong mixing claimed in Ref. [41]. The comparison with the trend of 2_1^+ levels suggests that the 0_2^+ levels are rather not double-phonon excitations. They are also not due to β vibrations, which are not expected in nuclei with spherical ground states ($N \leq 58$), whereas the 0_2^+ level at $N = 60$ has far too low an energy (we note that the existence of β vibrations in nuclei is being questioned [6,7,69–71]).

As mentioned, the 0_2^+ levels nuclei may result from excitations of nucleon pairs between neighboring orbitals. Figure 10(a) displays the Nilsson diagram for neutrons in the mass $A \approx 100$ region, showing the upsloping $\nu 9/2^+[404]$ extruder, which crosses a number of downsloping orbitals when the Fermi level rises between $N = 50$ and $N = 60$. We propose that a multiple action of the $\nu 9/2^+[404]$

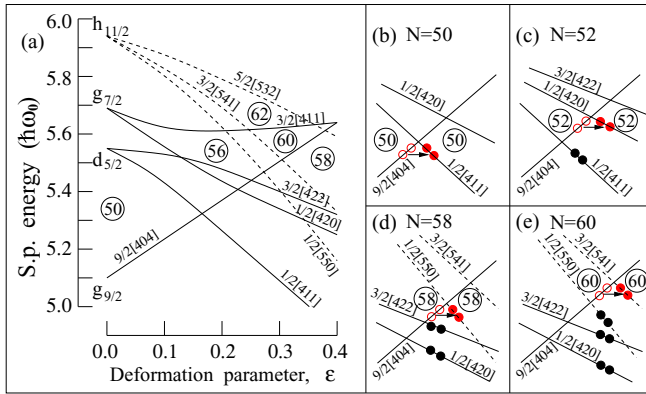


FIG. 10. (a) The Nilsson diagram for neutrons drawn after Fig. 9 of Ref. [55]. Panels (b)–(e) are described in the text.

extruder helps creating $2p$ - $2h$ excitations with spin 0^+ via the pair-hopping mechanism [10–12] as drawn schematically in Figs. 10(b)–10(e) showing fragments of Fig. 10(a) for various N values. An analogous mechanism was employed to explain the low-lying 0^+ levels in ^{98}Sr and ^{100}Zr [1] and in neutron-rich lanthanides where analogous extruders are the $\nu 11/2^-$ [505] and $\pi/2^+$ [404] orbitals [6–8].

At $N = 50$ [Fig. 10(b)], a neutron pair is passed from the occupied $9/2^+[404]$ to the empty $1/2^+[411]$ orbital, creating a 0^+ level at a rather high energy. With the increasing Fermi level and two neutrons added, the $9/2^+[404]$ orbital is filled again. The 0^+ ground state at $N = 52$ has the $\nu g_{9/2}$ shell fully occupied and two neutrons in the $d_{5/2}$ shell. However, at higher excitation another 0^+ level can be created by transferring a pair of neutrons from the $9/2^+[404]$ extruder to the $\nu 1/2^+[420]$ orbital as shown in Fig. 10(c). We note that the $1/2^+[411]$ orbital has properties of the $g_{7/2}$ shell after crossing with the $1/2^+[420]$ orbital and can interact with $g_{9/2}$ protons, lowering the excitation of the 0_2^+ level in ^{90}Sr .

The multiple action of the $\nu g_{9/2}$ extruder, a catalyst of the deformation-driving process, continues as long as it remains active at the Fermi level, crossing subsequent downsloping orbitals. The neutron pair transfer shown in Figs. 10(b) and 10(c) is repeated at higher N , building slowly the collectivity. However, at $N = 58$, there is an essential change as a pair of neutrons can be transferred to the *strongly* deformation-driving $1/2^-$ [550] orbital as shown in Fig. 10(d). This creates a deformed 0_2^+ level in ^{96}Sr . The deformation grows further at $N = 60$ where a pair of neutrons is passed to the $3/2^-$ [550] orbital as shown in Fig. 10(e). The interaction with $g_{9/2}$ protons lowers the energy of the 0_2^+ level such that it becomes the ground state in ^{98}Sr .

For the very low-lying spherical 0_2^+ level in ^{98}Sr a more exotic configuration was proposed with a pair of neutrons in the $11/2^-$ [505] orbital present at the Fermi surface on the oblate side of the potential (see Fig. 7 in Ref. [1]). This may explain some puzzling properties of this level—the very low mixing with the 0_1^+ ground state and numerous decays of the band on top of the 0_2^+ level to the ground-state band. The 0_3^+ level in ^{96}Sr may correspond to the same configuration (see Fig. 5 in Ref. [1]).

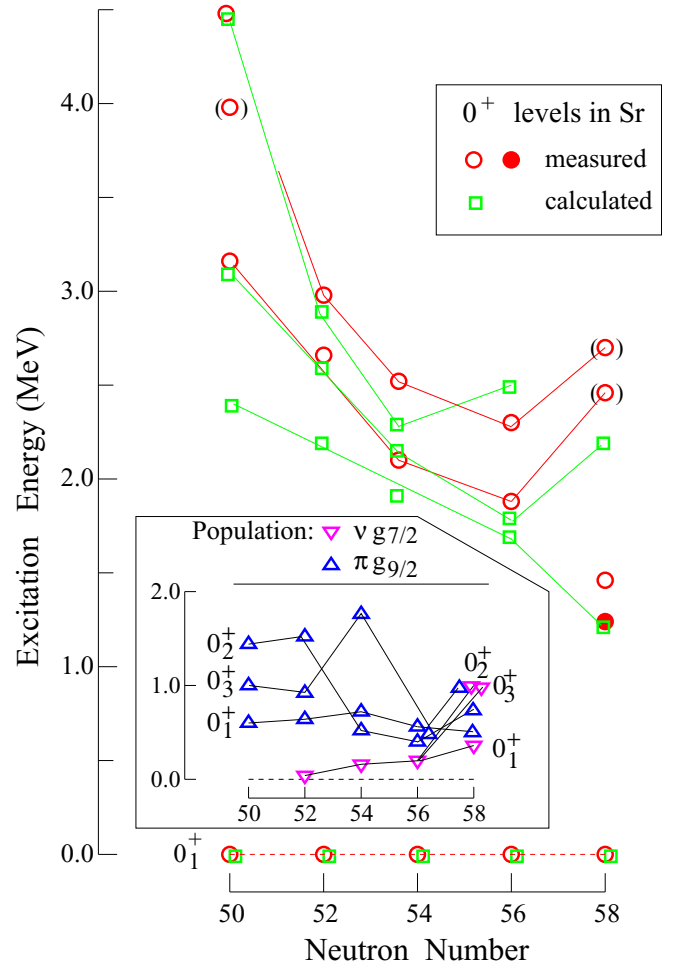


FIG. 11. Comparison of experimental and calculated excitation energies of 0_2^+ , 0_3^+ , and 0_4^+ levels in Sr isotopes. The filled circle represents a deformed state. The inset is described in the text. The data are taken from this paper and Ref. [4]. Lines are drawn to guide the eye.

Figure 11 compares measured energies of excited 0^+ levels in Sr isotopes with the corresponding energies obtained from the LSSM. The calculations reproduce the lowering of 0_{exc}^+ energies in the $50 \leq N \leq 56$ range. Curiously, the calculated 0_3^+ levels follow closely the experimental 0_2^+ levels whereas the calculated 0_2^+ levels seem not to have experimental counterparts. However, this may well be a mismatch between experiment and theory. An increase of calculated 0_{exc}^+ energies by about 0.5 MeV would give a fair agreement between 0_2^+ levels and a good match between 0_3^+ levels. To tell more, one should identify experimental 0_4^+ levels in $^{90,92,94}\text{Sr}$ nuclei, not known at present.

The situation at $N = 58$ needs special attention. As the 0_2^+ state in ^{96}Sr is supposed to be deformed, we do not expect it to appear in the present calculations due to a missing deformation-driving mechanism in the model space used. As inferred from previous calculations in Zr [61] and MCSM results [72], at $N = 58$ no deformed structures appear at low energy without addition of the intruders to the present valence

space. Also the 0_3^+ is suggested to be an exotic extruder-hole structure [1]. The calculated 0_2^+ and 0_3^+ fairly match the 0_3^+ and 0_4^+ experimental levels. The analysis of the wave functions of the computed, 0_2^+ and 0_3^+ levels at $N = 58$ shows low population of the SOP orbitals $\pi g_{9/2}$ and $\nu g_{7/2}$ (see the inset in Fig. 11), which suggests their spherical nature. This is in contrast with the predictions of the Monte Carlo SM calculations for the deformed states in the zirconium isotopes [72].

The main proton and neutron components in wave functions of levels from the LSSM calculations are named in Table XIV. For example, the proton component labeled “2” has six $\pi f_{5/2}$ protons, three $\pi p_{3/2}$ protons, one $\pi p_{1/2}$ proton, and no $\pi g_{9/2}$ protons. Analogously, the neutron component labeled “d” has four $\pi d_{5/2}$ neutrons and no neutrons in other shells.

The dominating components of 0^+ levels in Fig. 11 expressed in terms of Table XIV are shown in Table XV (we show components for which the probability in the wave function is, at least, 0.05). For example, the 0_2^+ level at $N = 54$ has two components $1d$ and $4d$ with probabilities of 0.12 and 0.38, respectively, accounting for 0.50 fraction of the wave function (this summed fraction is shown in the same line as the 0_2^+ symbol), the remaining 0.50 scattered among components with low amplitudes.

The most important features seen in Table XV are as follows:

(i) The complexity of wave functions increasing with growing neutron number. At $N = 50$, the probabilities of the few dominating components sum up to about 0.85, a fraction which drops below 0.5 at $N = 56$.

(ii) The domination of the $\nu d_{5/2}^n$ component $n=N-50$ in the wave functions at $N < 58$.

(iii) The domination of $\pi(f, p)$ components in the wave functions of the 0_1^+ level.

(iv) The increasing population of the $g_{9/2}$ proton orbital with excitation energy, and its decrease with the growing neutron number.

(v) Low population of the $g_{7/2}$ neutron orbital at $N < 58$.

The inset in Fig. 11 shows the summed population of the $\pi g_{9/2}$ and $\nu g_{7/2}$ shells. There is a moderate population of the $g_{9/2}$ proton and a very low population of the $g_{7/2}$ neutron shell (at $N < 58$, neutron population is very similar for 0_1^+ , 0_2^+ , and 0_3^+ levels). Although the occupancy of $\nu g_{7/2}$ and $\pi g_{9/2}$ orbitals increase at $N = 58$, it is still much below of what is expected in the highly deformed states (see Ref. [72]).

The above results indicate that the structure of excited 0^+ levels at $N < 58$ is dominated by the $\pi(f, p) \otimes \nu d_{5/2}^n$ configuration admixed by $g_{9/2}$ protons at higher energy but not by $g_{7/2}$ neutrons. Thus, the SOP mechanism does not work at $N < 58$, whereas the $\nu d_{5/2}^n$ component supports the extruder action shown in Figs. 10(b) and 10(c).

Finally, let us comment on other studies of 0^+ levels in Sr isotopes. The deformed band on top of the 0_2^+ level in ^{96}Sr , proposed in Ref. [33], was also reported by Coulomb-excitation studies [43,44] where, in addition, a deformed band on top of the 0_3^+ level at 1464.6 keV was suggested (not observed to date). In Ref. [45], a larger fraction of the spherical

TABLE XIV. The list of main proton and neutron components in wave functions of the levels in Sr isotopes as obtained in present LSSM calculations.

Proton component	$f_{5/2}$	$p_{3/2}$	$p_{1/2}$	$g_{9/2}$
			Positive	Parity
1	6	4	0	0
2	6	3	1	0
3	6	2	2	0
4	6	2	0	2
5	5	4	1	0
6	5	3	0	2
7	5	2	1	2
8	4	4	2	0
9	4	4	0	2
10	4	3	1	2
11	4	2	2	2
12	6	1	1	2
		Negative	Parity	
13	6	3	0	1
14	6	1	0	3
15	6	2	1	1
16	6	1	2	1
17	5	4	0	1
18	5	3	1	1
19	5	2	2	1
20	5	2	0	3
21	4	3	2	1

Neutron component	$d_{5/2}$	$s_{1/2}$	$g_{7/2}$	$d_{3/2}$	$h_{11/2}$
			Positive	Parity	
a	2	0	0	0	0
b	1	1	0	0	0
c	0	2	0	0	0
d	4	0	0	0	0
e	3	1	0	0	0
f	3	0	0	1	0
g	6	0	0	0	0
h	5	1	0	0	0
i	4	2	0	0	0
j	2	2	0	0	0
k	5	0	0	1	0
		Negative	Parity		
l	5	0	0	0	1
m	1	0	0	0	1
n	3	0	0	0	1

configuration was attributed to the 0_2^+ level than to the 0_3^+ level in ^{96}Sr , whereas the present paper suggests the opposite. It was also suggested that the 0_2^+ state in ^{98}Sr is similar to the 0_1^+ ground state in ^{96}Sr [46], albeit contradicting their shell-model calculations. As discussed above, we propose that the 0_2^+ level in ^{98}Sr is similar to the 0_3^+ level in ^{96}Sr . We agree with Ref. [46] that the Monte Carlo shell-model calculations [72] predict the onset of deformation in Sr isotopes at too low a neutron number. In Ru isotopes where the collectivity

TABLE XV. Structure of 0^+ levels in Sr isotopes in terms of main components listed in Table XIV as calculated with LSSM in this paper. See the text for further explanations.

Level	N = 50	N = 52	N = 54	N = 56
0_1^+	0.84	0.65	0.46	0.40
	1 , 0.59	1a , 0.33	1d , 0.20	1g , 0.12
	3 , 0.08	2a , 0.08	3d , 0.11	3g , 0.10
	4 , 0.11	3a , 0.11	4d , 0.05	8g , 0.18
	9 , 0.06	4a , 0.07	8d , 0.10	
		8a , 0.06		
0_2^+	0.86	0.50	0.50	0.45
	1 , 0.15	1a , 0.13	1d , 0.12	1g , 0.07
	3 , 0.05	4a , 0.19	4d , 0.38	8g , 0.38
	4 , 0.32	6a , 0.06		
	6 , 0.08	8a , 0.12		
	8 , 0.16			
	9 , 0.05			
	11 , 0.05			
0_3^+	0.83	0.62	0.32	0.49
	4 , 0.28	4a , 0.16	4d , 0.17	1g , 0.05
	8 , 0.55	8a , 0.41	4f , 0.06	1i , 0.05
		8c , 0.05	8d , 0.09	3g , 0.05
				8i , 0.34
0_4^+	0.81	0.62	0.29	0.06
	3 , 0.55	1c , 0.26	1j , 0.14	1g , 0.06
	7 , 0.09	2a , 0.13	8j , 0.15	
	8 0.17	3a , 0.06		
		8a , 0.06		
		8c , 0.06		
		9c , 0.05		

is higher than in Sr isotopes (see Fig. 1), a weakly deformed band on top of the 0_2^+ level was recently reported in $^{98}\text{Ru}_{54}$ [73].

C. 2^+ excitations

A low-energy 2_1^+ state, the most common type of excitation in nuclei is still an enigmatic phenomenon. As remarked in Ref. [71], “the phonon interpretation of the low-energy nuclear structure remains controversial.” In Ref. [12], the 2_1^+ excitations were called a “genuine quantum vibrations that are essentially different from surface oscillations of a classical liquid drop.”

Figure 12 displays low-energy positive-parity excitations as a function of the proton number Z . This picture and Fig. 8 show significant variations of 2_1^+ excitation energies along both Z and N . The 2_1^+ energy is nearly two times higher at $N = 50$ (no valence neutrons) than at $N = 52$. Furthermore, in $N = 50$ isotones, the 2_1^+ energy clearly increases at the $Z=40$ proton subshell closure, which is not seen at $N = 52$ where the pair of neutrons dilutes the effect (there is still a strong variation of the 0_2^+ energy at $N = 52$). Large variations of the 2_1^+ energy seen in Figs. 8 and 12 suggest that this is not any phonon-type excitation because a phonon, expected to be a complex excitation, should not show such rapid variations. Also the $R_{4/2}$ ratio of 2_1^+ and 4_1^+ excitation energies in the

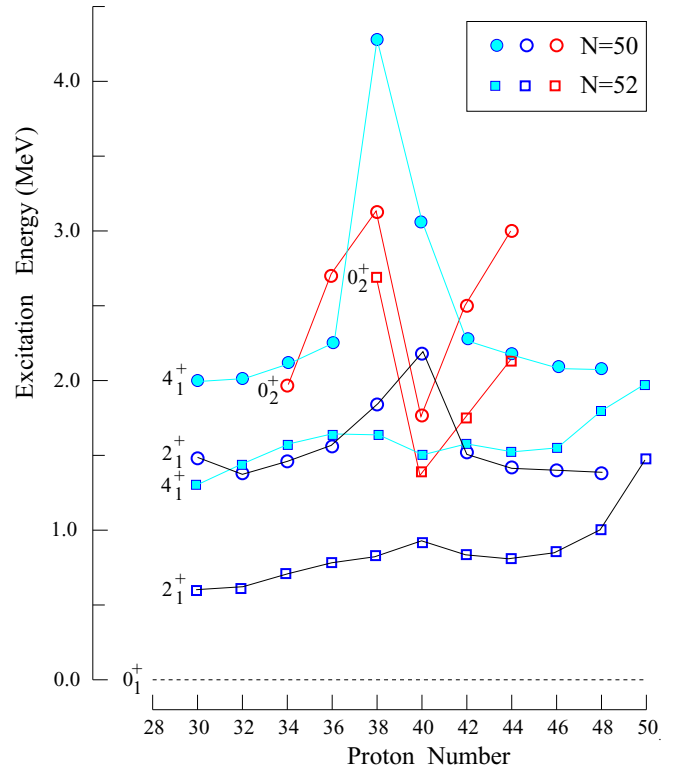


FIG. 12. Excitation energies of low-spin levels in $N = 50$ and $N = 52$ isotones. The data are from the present paper and from the ENSDF base [4]. Lines are drawn to guide the eye.

discussed nuclei does not support a two-phonon nature of the 4_1^+ levels shown. The figures indicate that both protons and neutrons contribute to these excitations and suggest that they are, predominantly, a few valence nucleons additionally “dressed in collectivity” [12] by coupling to a giant monopole, quadrupole and pairing vibrations [74–76]. Such coupling is supported by the observation that collectivity is fragmented among higher-lying 2^+ levels as seen in the neighboring Kr isotopes at $N = 50$ and $N = 52$ [77]. Low collectivity of 2_1^+ levels in $^{90-96}\text{Sr}$ isotopes is further indicated by small $B(E2; 2_1^+ \rightarrow 0_1^+)$ rates [78].

1. Structure of 2^+ levels

In Ref. [1], we proposed a phenomenological classification of 0^+ excitations where 57 out of 63 known 0_2^+ and 0_3^+ levels from the $38 \leq Z \leq 50$, $52 \leq N \leq 66$ region follow regular “parabolic” trends along the proton number. Analogous parabolas were obtained theoretically in the IBM-CM calculations of the intruder 0^+ levels in the region [68] (see Fig. 4 there).

Apparently, 2^+ excitations in Sr isotopes and their neighbors also can be arranged along ‘parabolas in the function of N , facilitating the understanding of various features shown in Fig. 8. Figure 13 shows three groups of such parabolas. We propose that each group corresponds to a specific proton configuration whereas the “U” shape within a group results from the Fermi level crossing a neutron shell. The regular trends seen in Fig. 13 involve 47 out of 53 known 2_1^+ , 2_2^+ , and

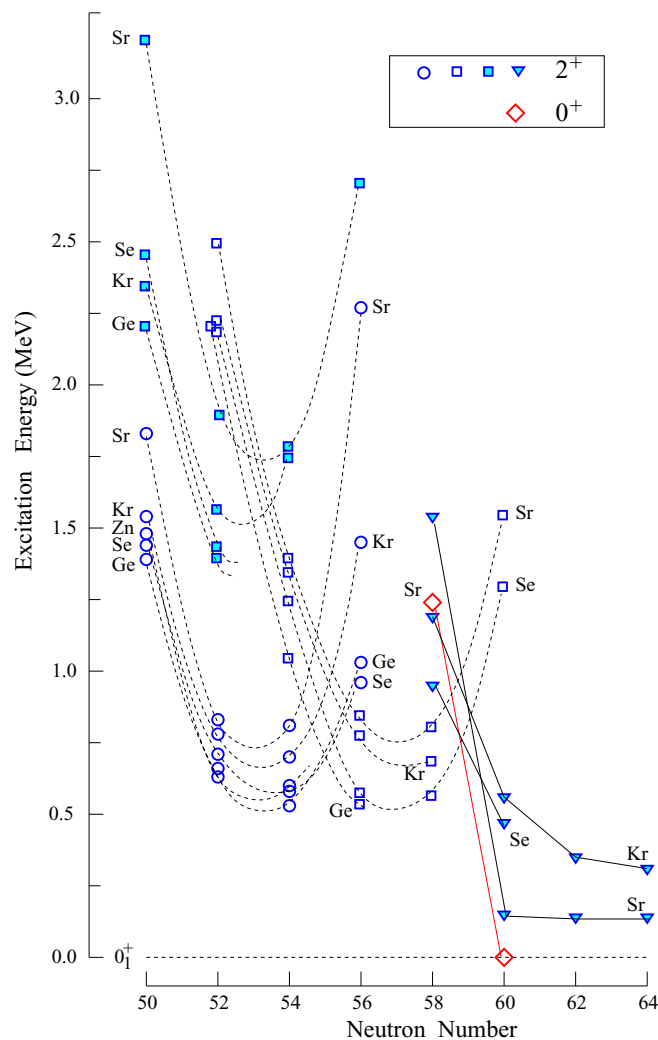


FIG. 13. Excitation energies of 2_1^+ , 2_2^+ , and 2_3^+ levels in Zn, Ge, Se, Kr, and Sr isotopes. The data are taken from the present paper and from the ENSDF base [4]. Lines are drawn to guide the eye. See the text for further comments.

2_3^+ levels in the ($32 \leq Z \leq 38$, $50 \leq N \leq 60$) region. The six remaining cases are discussed below.

We propose that the 2^+ levels represented by open circles correspond to excitations within the $d_{5/2}$ neutron shell. In the $50 \leq N \leq 54$ range, these points correspond to 2_1^+ levels, but when the Fermi level approaches $N = 56$, energies of these levels increase, and they become 2_2^+ excitations. It is expected that the proton configuration in this group has the lowest energy. Filled squares may correspond to the same neutron configuration coupled to a higher-energy proton excitation. The points represented by open squares, being 2_1^+ levels at $N = 56$ and $N = 58$, 2_2^+ excitations at $N = 54$ and 2_3^+ excitations at $N = 52$, may correspond to filling other neutron shells.

To learn more, we performed LSSM calculations for 2^+ excitations in Sr isotopes. Figure 14 compares measured and calculated energies of 2_1^+ , 2_2^+ , and 2_3^+ levels in $^{88,90,92,94,96}\text{Sr}$ nuclei. The calculated points follow closely the experimental “parabolic” trends. In the figure, there are four distinct groups

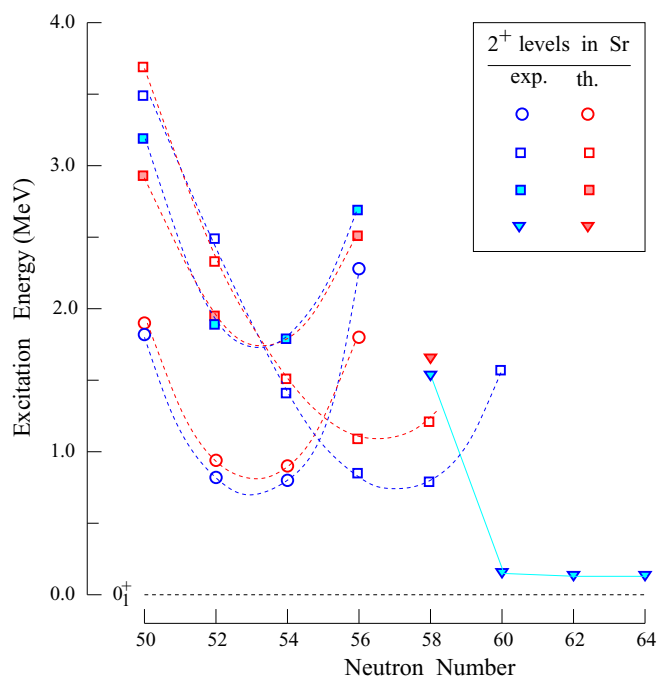


FIG. 14. Comparison of excitation energies of 2_1^+ , 2_2^+ , and 2_3^+ levels in Sr isotopes observed experimentally (blue symbols) and calculated within the LSSM (red symbols). The data are taken from the present paper and from the ENSDF base [4]. Lines are drawn to guide the eye.

of data points. One may ask whether the LSSM calculations predict similar configurations within each groups.

Dominating structures of the configurations in Fig. 14, calculated at $N = 50, 52, 54$, and 56 are shown in Table XVI. For each configuration, we show the most important components for which the probability in the wave function is, at least, 0.05. For example, the 2_1^+ level at $N = 54$ has three components, $1d$, $2d$, and $3d$ with probabilities of 0.17, 0.07, and 0.10,

TABLE XVI. The structure of 2_1^+ , 2_2^+ , and 2_3^+ levels in Sr isotopes in terms of components listed in Table XIV as calculated with the LSSM in this paper. See the text for further comments.

Level	$N = 50$	$N = 52$	$N = 54$	$N = 56$
2_1^+	0.76	A , 0.53	A , 0.34	B , 0.23
	2 , 0.34	1a , 0.28	1d , 0.17	2g , 0.08
	5 , 0.35	2a , 0.14	2d , 0.07	5g , 0.09
	8 , 0.07	3a , 0.11	3d , 0.10	8g , 0.06
2_2^+	0.89	0.49	B+A , 0.42	B+A , 0.41
	2 , 0.38	1a , 0.05	2d , 0.16	1h , 0.05
	5 , 0.39	1b , 0.09	3d , 0.05	5g , 0.10
	7 , 0.06	2a , 0.15	5d , 0.16	8g , 0.10
2_3^+	0.71	A+B , 0.44	0.40	0.31
	4 , 0.60	1a , 0.05	1e , 0.17	2g , 0.13
	6 , 0.05	1b , 0.17	8e , 0.11	5g , 0.05
	9 , 0.06	2a , 0.05	2d , 0.06	8h , 0.13
		5a , 0.17	3e , 0.06	

respectively, which sum up to 0.34. We note that this configuration has a simple structure of dominating components, which can be written as $(1 + 2 + 3) \otimes \nu d_{5/2}^n$, where $n = N - 50$. We assign label A to this configuration. It describes 2_1^+ levels at $N = 52$ and $N = 54$. Analogously, configuration B assigned to the 2_1^+ level at $N = 56$ in Table XVI can be written as $(2 + 5 + 8) \otimes \nu d_{5/2}^n$.

At higher excitation energies, the configurations mix and acquire more components with lower amplitudes. Notably, the 2_2^+ levels at $N = 54$ and $N = 56$ are mixtures of configurations A and B. A remarkable result of this paper is the demonstration that the crossing in the experimental systematics of excitation energies between configurations A and B (blue circles and squares on blue parabolas in Fig. 14) is reproduced by the calculated structures of the corresponding 2^+ levels. The 2_1^+ level, which has the configuration A at $N = 52$ and $N = 54$ (red circles), changes its structure to configuration B (red square) at $N = 56$, whereas the 2_2^+ level, which has the dominating configuration B at $N = 54$ (red square) acquires an admixture of configuration A at $N = 56$ (red circle). This explains the “unusual” position of the 2_2^+ level of ^{96}Sr in Fig. 8.

It is of interest to extend such shell-model analysis to 2^+ levels in other isotopic lines displayed in Fig. 13, showing experimental systematics similar to those of Sr isotopes.

2. 2_1^+ levels and the deformation

Figure 13 reveals another interesting effect. The points shown by filled triangles correspond to 2^+ excitations in rotational bands and display trend (seen most clearly in Sr isotopes) where the 2_2^+ level rapidly drops in energy (from 1507.0 keV in ^{96}Sr to 144.6 keV in ^{98}Sr) and continues as the 2_1^+ rotational level (positions of corresponding 0^+ band heads are marked by red diamonds). The 2_1^+ levels at $N \geq 60$ and 2_2^+ levels in ^{92}Se and ^{94}Kr at $N = 58$, shown by filled triangles, belong to the same category. One notes, that the 2_1^+ energy in ^{94}Se is lower than in ^{96}Kr . Thus, the collectivity in Se isotopes may be higher than in Kr isotopes, contrary to claims of Ref. [79] that Kr isotopes mark the low- Z boundary of the deformation at $N = 60$ (it is of a high interest to find the 2_1^+ excitation energy in $^{96}\text{Se}_{62}$). This is supported by Ref. [62] (see Fig. 1 there) suggesting an increase in collectivity below $Z=36$. As noted there the tensor mechanism proposed in Ref. [72] does not work at $Z < 38$, so the collectivity should have another origin.

The evolution in Kr isotopes seen in Fig. 13 is characteristic of the second-order phase transition [80,81] where the 2_1^+ energy drops gradually, and there is no crossing with a deformed 0_2^+ configuration. More generally, the deformation change around the neutron number $N = 60$ corresponds primarily to the second-order phase transition (gradual increase in collectivity in the ground-state configuration with the increasing neutron number) and is observed in a wide range of protons from Se (possibly Ge) to Pd with maximum collectivity in Mo isotopes. However, on top of this change superimposed is another contribution to the shape change, which is due to the first-order phase transition [80,81], helped here by the $\nu 9/2^+[404]$ extruder, generating coexist-

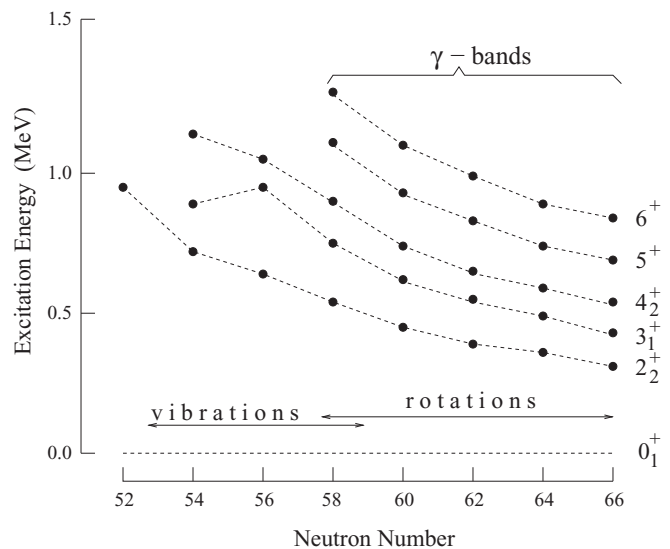


FIG. 15. Evolution of γ bands in Ru isotopes. Data are taken from Ref. [3] and the ENSDF base [4].

ing deformed 0^+ configurations in Sr and Zr [1]. The two contributions added are responsible for a sudden deformation onset observed at $N = 60$ in ^{98}Sr and ^{100}Zr nuclei. This picture is supported by the evolution of the mean-square charge radii and the two-neutron separation energies in the region [68,82,83], which are sensitive probes of collectivity [84–86]. As seen in Fig. 1 of Ref. [82], Fig. 2 of Ref. [68], and Figs. 3 and 4(a) of Ref. [83], there is an extra variation of these two observable in Rb, Sr, Y, Zr, and Nb isotopes around neutron number $N = 59$, which is where the $9/2^+[404]$ neutron extruder is observed at the Fermi level [48,55,59,60,87–91].

D. γ vibrations vs mixed-symmetry states

The so-called γ excitations, which are 2^+ levels with $K=2$ projection on the symmetry axis, are commonly reported at low energies. In many nuclei, they are identified with 2_2^+ levels and are believed to be collective modes with bands on top of them. The most spectacular γ bands in the region are reported in Mo [92] and Ru nuclei [93] with the best-to-date candidate for a harmonic two-phonon γ -vibrational state in ^{106}Mo [94]. In spherical nuclei with no symmetry axis defined, the $K=2$ excitations are not expected. Still one observes there 2^+ levels, which evolve smoothly into γ bands at higher N as illustrated in Fig. 15 for Ru isotopes.

Apart from the $K=2$ projection, another specific feature of a γ band is the 3^+ excitation within the band. Its position relative to the 2^+ and 4^+ in-band levels allows distinguishing between vibrational or rotational character of the band [95–97], although with some doubts [98].

Numerous 3^+ levels in the region were reported [63,64,99] with the recent example of both vibrational and rotational γ bands in ^{100}Zr and ^{102}Z [100]. The data from Fig. 8 of Ref. [64], including 3^+ levels from excitation schemes in Figs. 3, 5, 7, are shown in Fig. 16 for the $N = 52, 54, 56,$ and 58 isotones. In the figure, we also show 2^+ excitations,

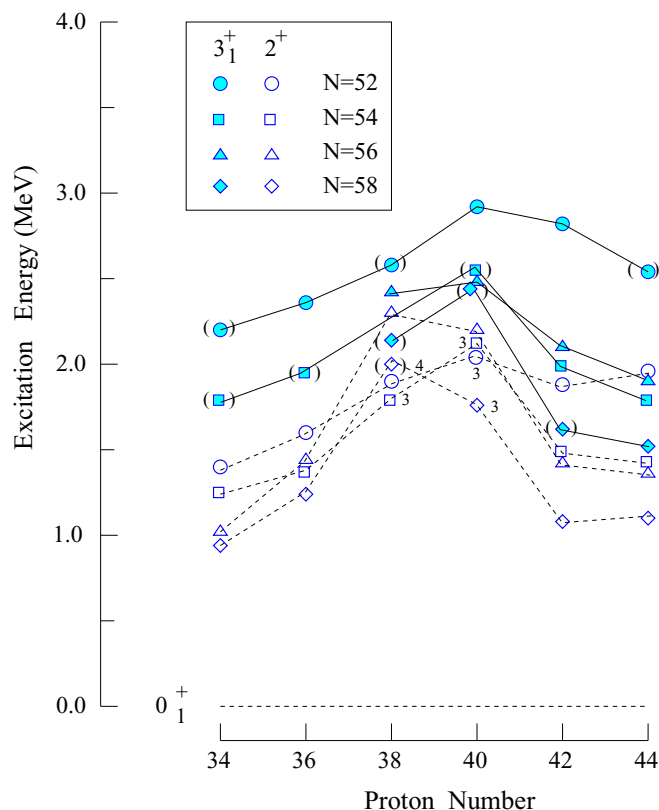


FIG. 16. Excitation energies of 3_1^+ (filled symbols) and related 2^+ (empty symbols) levels in $N = 52, 54, 56,$ and 58 isotones. In five cases, the 2_3^+ and 2_4^+ levels are shown. Data with nonunique spin-parity assignments are shown in parentheses. The data are taken from this paper and Refs. [4,63,64,99].

which are related to 3^+ levels. In most cases, these are 2_2^+ levels but for ^{92}Sr , ^{92}Zr , ^{94}Zr , and ^{98}Zr where the 2_2^+ level is not connected with the 3^+ level, we have shown 2_3^+ levels and in ^{96}Sr , the 2_4^+ level.

All four isotonic lines show similar patterns with 2^+ and 3^+ energies increasing with the growing proton number up to $Z=38$ or $Z=40$ and then decreasing. Both 2^+ and 3_1^+ energies decrease with the growing neutron number. These similarities and regularities suggest that the levels shown in Fig. 16 belong to the same excitation mode, which in Mo and Ru nuclei is identified as γ excitation.

In Fig. 17, the calculated energies of 3_1^+ levels in Sr isotopes are compared to their experimental counterparts. We show, in addition, experimental levels for Mo and Ru isotopes, where 3_1^+ levels are identified as members of γ bands. The similarity between systematic trends shown by the Sr, Mo, and Ru data along N suggests that the 3_1^+ levels in Sr isotopes have similar structures as those in Mo and Ru isotopes. This is in contrast to the shell-model calculations of Ref. [41] where it was concluded that the 3_1^+ level at 2421.50 keV in $^{94}\text{Sr}_{56}$ is predominantly a single-particle excitation.

The calculated excitation energies (red circles) follow closely the experimental data. In ^{92}Sr where the experimental

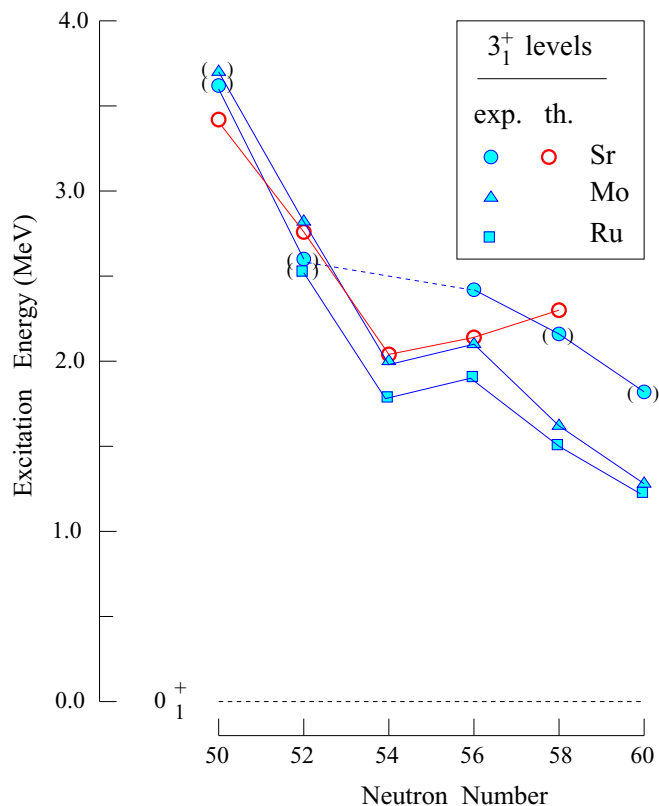


FIG. 17. Experimental excitation energies of 3_1^+ levels in the $50 \leq N \leq 58$ isotopes of Sr (filled blue circles) compared to the LSSM calculated energies (empty red circles). Experimental energies for 3_1^+ levels in isotopes of Mo (filled blue triangles) and Ru (filled blue squares) are shown for comparison. Data points with nonunique or tentative spin-parity assignments are shown in parentheses. The experimental data are taken from the present paper and the ENSDF base [4].

3_1^+ level is not known, the calculations predict an excitation energy of 2.05 MeV, in accord with the downsloping trend in Mo and Ru.

We have also checked the quadrupole properties of the calculated 3_1^+ levels in the Sr chain. In ^{92}Sr , the spectroscopic quadrupole moment $Q(3_1^+) = 2.2e^2 \text{fm}^2$ approaches the zero value expected for a $K_1 = 2$ band. Furthermore, the 3_1^+ and the second excited 2_2^+ state are connected by a strong $E2$ transition of $B(E2; 3^+ \rightarrow 2_2^+) = 319e^2 \text{fm}^4$ [for comparison, $B(E2; 2^+ \rightarrow 0_{g.s.}^+) = 224e^2 \text{fm}^4$]. This and the lowering of the computed 3_1^+ energy as a function of N suggests some nonaxiality at $N = 54$. It is worth noting that the same LSSM calculations predicted triaxial deformation in Se and Ge isotopes with $N = 52, 54$ [101].

In Table XVII, structures of calculated 3_1^+ levels in Sr isotopes are expressed in terms of dominating components. Comparing structures of 3^+ levels from Table XVII with structures of 2^+ levels from Table XVI, one sees that the dominating components in wave functions of 3_1^+ levels are closer to those of 2_2^+ levels than of other 2^+ levels. The systematic trend in Fig. 17 even resembles the crossing between two parabolas for 2_2^+ and 2_3^+ levels in Fig. 14 with the 3_1^+ configurations at

TABLE XVII. Structure of 3^+ levels in Sr isotopes in terms of main components listed in Table XIV as calculated with the LSSM in this paper. See the text for further comments.

Level	N = 50	N = 52	N = 54	N = 56
3_1^+	0.93	0.61	0.54	0.50
	5 , 0.81	1b , 0.15	1d , 0.20	1h , 0.11
	7 , 0.06	2a , 0.17	2d , 0.09	3h , 0.09
	10 , 0.06	2b , 0.07	3d , 0.12	8h , 0.30
		5a , 0.11	8d , 0.13	
		5b , 0.06		
		8b , 0.05		
3_2^+		0.53	0.37	0.26
		1b , 0.23	5d , 0.11	1k , 0.12
		2a , 0.09	8d , 0.06	3k , 0.06
		5a , 0.14	1e , 0.11	8k , 0.08
		8b , 0.07	8e , 0.09	

$N = 52$ and $N = 54$ having more low amplitude components than at $N = 50$ and $N = 56$, which may reflect configuration mixing at the crossing. Indeed, the 3_2^+ level at 2.92 MeV (0.15 MeV above 3_1^+) in $^{90}\text{Sr}_{52}$ has a very similar structure to the structure of 3_1^+ levels in ^{90}Sr and ^{92}Sr .

Interestingly, at $N = 56$, the 3_2^+ state predicted at 2.86 MeV is dominated by a neutron excitation to the $d_{3/2}$ orbital whose *total* occupation reaches 0.77 particle. The same population of the $d_{3/2}$ orbital is predicted in the 3_1^+ level at $N = 58$ where in addition the total occupation of the $g_{7/2}$ orbital grows to 0.6. However, the sum of the dominating components is 0.32 only indicating a continuous increase in collectivity with N . At the same time, the proton structure of the 3^+ levels remains nearly unchanged along the chain with the $g_{9/2}$ occupation around 0.5 particle. As for 2^+ levels, the total population of the $\nu g_{7/2}$ shell in 3^+ levels at $N < 58$ is negligible.

The observed proximity of two 3^+ configurations is expected in this region where apart from γ -excitation mixed-symmetry states 2_m^+ , which are proton-neutron isovector excitations [102–104], are reported at $N = 52$ and $N = 54$ in ^{92}Zr [105], ^{94}Mo [106–109], $^{96,98}\text{Mo}$ [110], and ^{96}Ru [111]. The quadrupole collective mode Q_m , generating mixed-symmetry states, coupled to the 2_1^+ state (the symmetric Q_s mode) produces a quintuplet of two-phonon states $Q_m Q_s |0_1^+\rangle$ with spins from 0^+ to 4^+ , which decay by enhanced M1 transitions to 0^+ , 2^+ , and 4^+ states of the two-phonon symmetric triplet $(Q_s Q_s)$.

The characteristic signature of the $Q_m Q_s |0_1^+\rangle$ quintuplet is the low-energy 1^+ excitation. Figure 18 shows known experimental levels with spin 1^+ in Sr isotopes with $50 \leq N \leq 58$. For comparison, we show 1^+ levels in Zr, Mo, and Ru isotopes. There is a general decrease in 1^+ excitation energies with the growing neutron number. The LSSM calculations shown in Fig. 18, reproduce well the 1^+ energy in $^{88}\text{Sr}_{50}$ and are close to 1^+ energies in Zr, Mo, and Ru nuclei at $N = 52$ (experimental 1^+ level in $^{90}\text{Sr}_{52}$ is not known). The trend in Fig. 18 resembles the trend of 3_1^+ levels in Fig. 17, suggesting some relation between 1_1^+ and 3_1^+ states.

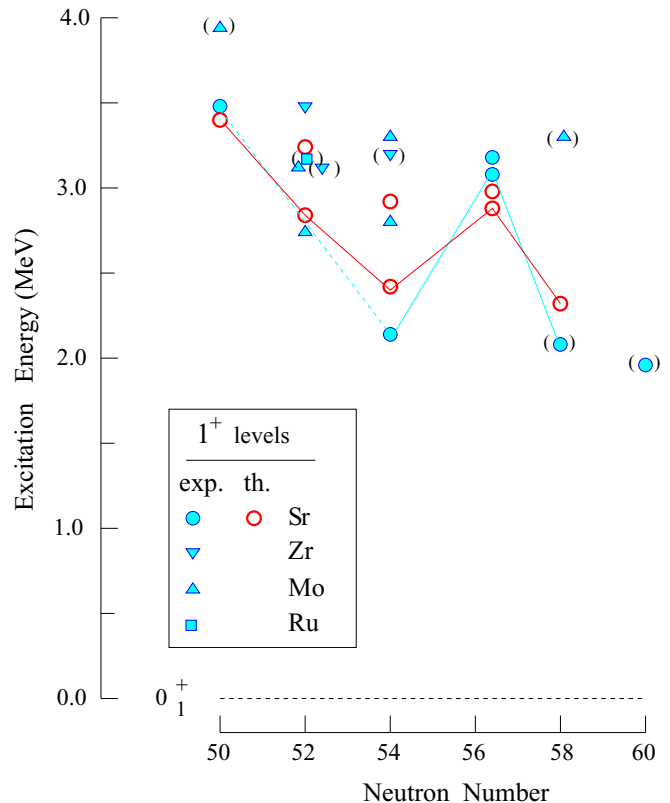


FIG. 18. Experimental excitation energies of 1^+ levels in the $50 \leq N \leq 58$ Sr isotopes compared to the LSSM calculated energies. Experimental 1^+ levels in isotopes of Zr, Mo, and Ru are shown for comparison. The data with tentative spin-parity assignments are shown in parentheses. The experimental data are taken from the present paper and Ref. [4].

However, 1^+ states may have another origin. The 1^+ excitation with enhanced M1 decay seen in $^{86}\text{K}_{50}$ [57] does not involve valence neutrons. As discussed in the review work [112], 1^+ excitations may appear due to coupling with high-energy modes. Furthermore, as argued in Ref. [61], the LSSM calculations produce more complex wave functions in these nuclei than expected for a pure $Q_s |0_1^+\rangle$, $Q_m |0_1^+\rangle$ state. One may also note that at $N = 50$, the 1_1^+ energy in ^{88}Sr is significantly lower than in ^{90}Zr (4.6 MeV) and is close to that in ^{86}Kr (2926 keV). This suggests that below $Z=40$, the 1_1^+ levels at $N = 50$ are due to s-p. proton excitations within $\pi(f, p)$ shells.

Figure 19, which is analogous to Fig. 17 of Ref. [57], shows, in panel (a), low-spin levels in ^{88}Sr drawn after the compilation [113] and, in panel (b), a schematic decay pattern between mixed-symmetry (Q_m , $Q_m Q_s$) and symmetric (Q_s , $Q_s Q_s$) excitations, dominated by strong M1 transitions [102]. As in case of ^{86}Kr , basic components of the pattern shown in Fig. 19(b) are present in Fig. 19(a) (although with rather high energies of $Q_s Q_s$ states).

Table XVIII shows the LSSM configurations for 1^+ levels in Sr isotopes. At $N = 50$, a few single-particle excitations constitute about 90% of wave functions, but the dominating $\pi(f, p)$ configurations are different than in 3^+ levels. In

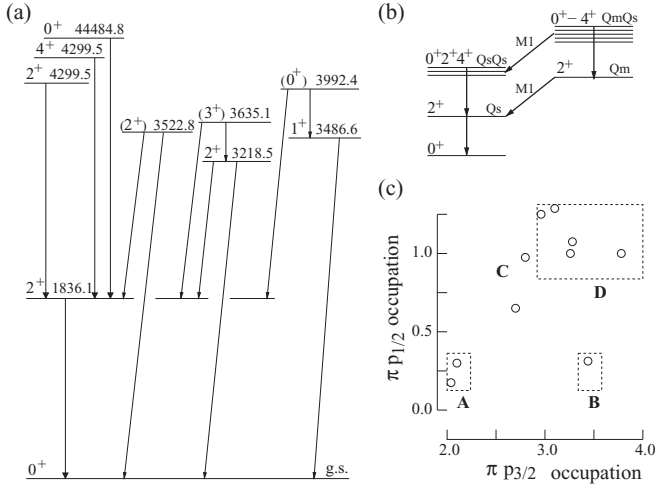


FIG. 19. (a) Partial scheme of low-spin excitation in ^{88}Sr drawn after the compilation [113], (b) a schematic of decays between mixed-symmetry and symmetric excitations, and (c) occupation of $\pi p_{3/2}$ and $\pi p_{1/2}$ orbitals calculated for levels of ^{88}Sr . The A–D labels are explained in the text.

contrast, at $N = 52$, single-particle excitations have a similar $\pi(f, p)$ configuration in 1_1^+ and 3_1^+ levels. This suggests the proton-neutron mixed-symmetry excitations in $^{90}\text{Sr}_{52}$. The properties of ^{88}Sr suggest that the skeleton of this pattern is formed at $N = 50$ by single-particle excitations and then additionally dressed by the mixed-symmetry collectivity at $N = 52$.

Table XIX shows $B(M1)$ transition rates obtained from the LSSM for transitions between low-spin excitations in ^{88}Sr and ^{90}Sr . The 2_2^+ level in ^{90}Sr could be identified as a mixed symmetric due to its high $B(M1; 2_2^+ \rightarrow 2_1^+)$ value and a relatively low $B(E2; 2_2^+ \rightarrow 0_1^+) = 48e^2\text{fm}^4$. Nonetheless, the remaining $B(M1)$ s are not supporting the mixed-symmetry character of any other of the excited states. The LSSM calculation suggests the dominating single-particle character of the 1^+ and 3^+ levels in ^{88}Sr with some admixture of quadrupole collectivity at $N = 52$.

As shown in Fig. 19(c), the occupation of $\pi p_{1/2}$ and $\pi p_{3/2}$ orbitals is correlated in the $\pi p_{1/2}$ vs $\pi p_{3/2}$ plane, similarly as observed in ^{86}Kr . By analogy to Fig. 17(b) of Ref. [57], we

TABLE XVIII. Structure of 1^+ levels in Sr isotopes in terms of components from Table XIV as obtained in this paper.

Level	N = 50	N = 52	N = 54	N = 56
1_1^+	0.97	0.64	0.47	0.46
	2 , 0.78	2a , 0.25	1e , 0.19	2h , 0.06
	7 , 0.07	5a , 0.32	2e , 0.08	5h , 0.25
	10 , 0.06	8a , 0.07	3e , 0.07	8h , 0.15
	12 , 0.06		8e , 0.13	
1_2^+	0.84	0.57	0.44	0.36
	4 , 0.69	2a , 0.50	2d , 0.27	2g , 0.30
	6 , 0.08	5a , 0.07	8d , 0.06	1k , 0.06
	12 , 0.07		1f , 0.06	

TABLE XIX. $B(M1)$ values (in μ_N^2 units) for selected transitions in ^{88}Sr and ^{90}Sr obtained in the LSSM calculations.

$J_f^\pi \rightarrow J_i^\pi$	$B(M1; ^{88}\text{Sr})$	$B(M1; ^{90}\text{Sr})$
$2_2^+ \rightarrow 2_1^+$	0.06	0.17
$2_3^+ \rightarrow 2_2^+$	0.013	0.07
$3_1^+ \rightarrow 4_1^+$	0.35	0.0004
$1_1^+ \rightarrow 2_2^+$	0.05	0.05
$1_1^+ \rightarrow 2_3^+$	0.04	0.075

distinguish, in Fig. 19(c), four groups of data points, labeled A–D (group C is less distinct here than in ^{86}Kr). Table XX shows occupation probabilities of proton orbitals in low-spin levels of ^{88}Sr . Labels A–D are assigned to the respective levels in Table XX) to facilitate the comparison with analogous occupations in ^{86}Kr , shown in Table X of Ref. [57]. The correlated populations of $\pi p_{1/2}$ and $\pi p_{3/2}$ proton shells produce, at $N = 50$, an excitation pattern shown in Fig. 19(a), which is the skeleton for mixed-symmetry excitations. At $N > 50$, it acquires some extra collectivity due to p-n coupling.

E. Negative-parity excitations in Sr isotopes

Figure 20 shows excitation energies of 3^- and 5^- levels in Kr, Sr, Zr, and Mo isotopes of the region, revealing some systematic trends. Excitation energies of 3_1^- levels decrease with the increasing neutron number in all the nuclei shown. This suggests an increase in octupole correlations with the increasing neutron number. However, as seen in Figs. 5 and 7, the population of negative-parity levels in ^{96}Sr is lower than in ^{94}Sr , and the 3^- level is not known in ^{98}Sr , which may be, partly, due to its nonyrast character increasing with N .

In addition to the isoscalar octupole phonon observed in the region [114], the isovector 3^- excitation [115] as well as s.-p. configurations of negative parity appear at similar energies. For example, 5_1^- levels in ^{90}Zr and ^{92}Mo were interpreted as the proton $(g_{9/2}p_{1/2})_{5^-}$ s.-p. coupling, and Fig. 20 shows more such levels (points connected by the dashed lines). Their excitation energies increase with the increasing neutron number, in contrast to other 5^- levels, which probably correspond to

TABLE XX. Occupation of proton orbitals in selected levels of ^{88}Sr . See the text for more comments.

I^π	$E_{\text{exc}}(\text{keV})$	$f_{5/2}$	$p_{3/2}$	$p_{1/2}$	$g_{9/2}$	Group
0_1^+	0	5.64	3.44	0.31	0.62	B
2_1^+	1892	5.21	3.28	1.08	0.43	D
0_2^+	2374	5.21	2.70	0.64	1.44	C
2_2^+	2945	5.32	3.26	1.01	0.42	D
0_3^+	3013	4.59	3.11	1.29	1.01	D
1_1^+	3209	5.77	2.80	0.98	0.45	C
3_1^+	3416	4.86	3.78	1.00	0.36	D
2_3^+	3713	5.56	2.08	0.29	2.07	A
4_1^+	3961	4.73	2.97	1.26	1.04	D
2_4^+	4065	5.49	2.22	0.43	1.86	A
4_2^+	4367	5.45	1.98	0.17	2.10	A

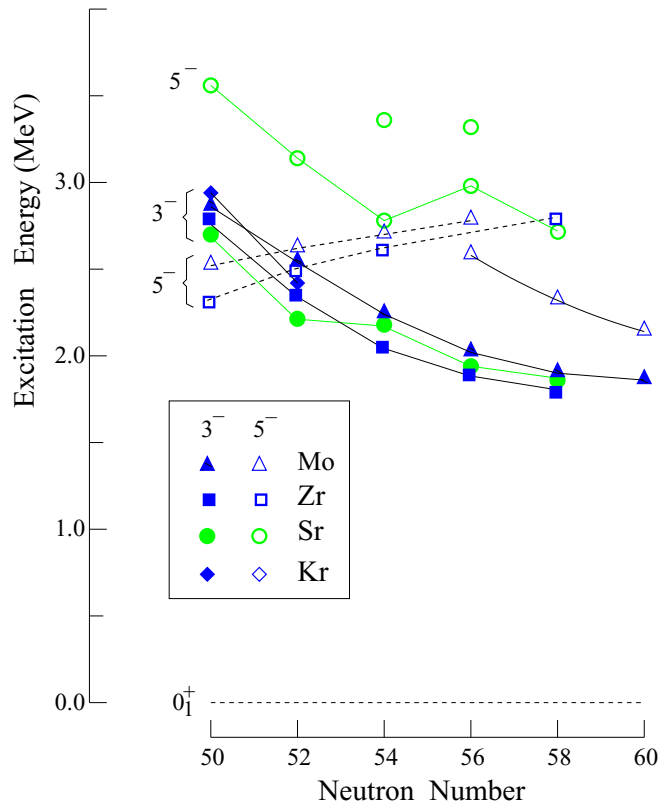


FIG. 20. Experimental excitation energies of negative-parity levels in Sr isotopes compared to the LSSM calculations. The data are taken from this paper and the ENSDF base [4].

the $2^+ \otimes 3^-$ coupling. The 5_1^- levels in Sr isotopes show an irregular trend, and it is not obvious to which configuration they belong—there are close-lying 5_2^- levels in ^{92}Sr and ^{94}Sr , and it is possible that the two configurations mix.

Figure 21 compares experimental excitation energies of low-spin negative-parity levels in Sr isotopes in the $50 \leq N \leq 58$ range (filled, green symbols) with energies obtained in the LSSM calculations (empty, red symbols). The LSSM results reproduce the observed excitation energies on average with the exception of 3^- states for which the theory predicts strong increase of their excitation energy with N . This suggests an octupole collectivity setting in towards heavier isotopes, which cannot be accounted for by the present calculations. Indeed, all calculated energies increase at the $N = 56$ subshell closure, which suggests that the calculated levels are of a more single-particle character than experimental levels.

The dominating components of the corresponding wave functions obtained from LSSM are shown in Table XXI. The calculated configurations are dominated by a few components, although their summed contribution drops with N . One notes the increase in negative-parity neutron components at higher N . Another effect is the increasing contribution of dominating components with growing spin, seen at $N = 56$. The inset in Fig. 21 shows the total population of the $\pi g_{9/2}$ and $\nu h_{11/2}$ unnatural-parity shells. This population supports the single-particle character of the 9_1^- level in the region [18] with the $\nu h_{11/2}$ contribution increasing with N .

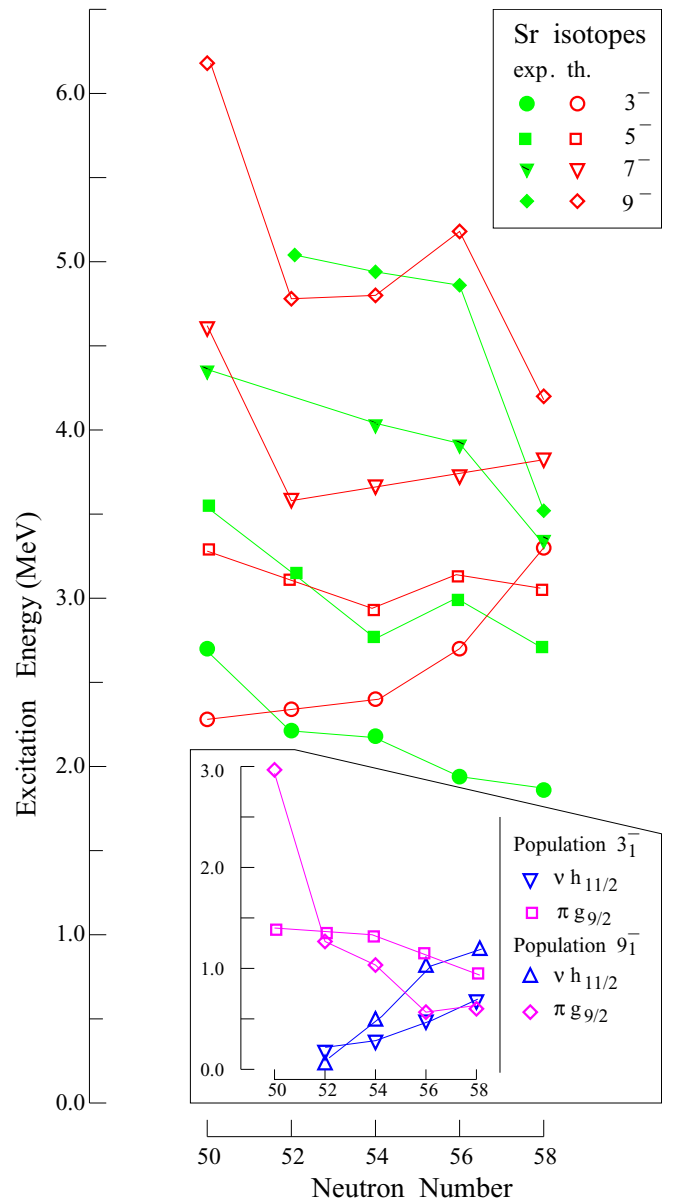


FIG. 21. Experimental energies of negative-parity states (filled green symbols) vs the LSSM calculated energies (empty red symbols) in Sr isotopes. The inset is described in the text. The data are from this paper and the ENSDF base [4].

In the discussed region, one observes negative-parity excitations above the 9_1^- level. They correspond to fully aligned two- or four-quasiparticle configurations, providing information on high- j orbitals. The example is the 17^- level in ^{98}Zr corresponding to the $[\pi(g_{9/2})^2 \otimes \nu(g_{7/2}h_{11/2})]_{17^-}$ configuration [61,116]. In the present paper, we observe cascades on top of the $\nu(g_{7/2}h_{11/2})_9^-$ configuration in ^{94}Sr and ^{96}Sr . They have higher excitation energies than analogous levels in Zr isotopes due to the higher $\pi g_{9/2}$ energy at $Z=38$ than at $Z=40$.

F. Medium-spin positive-parity excitations in Sr

The lowest two-q.p. fully aligned excitations of positive parity in the discussed nuclei correspond to the $(g_{9/2})_8^+$ and

TABLE XXI. Structure of negative-parity levels in Sr isotopes in terms of dominating components listed in Table XIV as calculated with the LSSM in this paper.

I^π	N = 50	N = 52	N = 54	N = 56
3_1^-	0.84 13 , 0.71 14 , 0.08 20 , 0.05	0.51 13a , 0.38 15a , 0.08 1m , 0.05	0.39 13d , 0.23 15d , 0.06 16d , 0.05 1n , 0.05	0.37 13g , 0.13 16g , 0.05 21g , 0.07 1l , 0.07 8l , 0.05
4_1^-	0.81 13 , 0.62 15 , 0.06 17 , 0.13	0.62 13a , 0.34 15a , 0.11 17a , 0.10 18a , 0.07		
5_1^-	0.80 13 , 0.75 15 , 0.05	0.55 13a , 0.43 15a , 0.12	0.31 13d , 0.21 15d , 0.10	0.16 1l , 0.06 3l , 0.05 8l , 0.05
6_1^-	0.77 13 , 0.27 17 , 0.45 20 , 0.05	0.59 13a , 0.11 17a , 0.28 18a , 0.11 19a , 0.09	0.37 13d , 0.06 17d , 0.17 18d , 0.06 19d , 0.08	0.13 17g , 0.07 19g , 0.06
7_1^-	0.90 17 , 0.64 18 , 0.05 19 , 0.08 20 , 0.07 22 , 0.06	0.57 13a , 0.51 15a , 0.07 1m , 0.16	0.35 13d , 0.07 13n , 0.06 1n , 0.15 3n , 0.07	0.33 1l , 0.13 3l , 0.09 8l , 0.11
9_1^-	0.98 14 , 0.81 20 , 0.17	0.64 13a , 0.51 15a , 0.05 17a , 0.08	0.28 13d , 0.07 17d , 0.07 1n , 0.09 13n , 0.05	0.34 2l , 0.13 5l , 0.16 8l , 0.05

$(f_{5/2})_{4+}^2$ proton as well as the $(d_{5/2})_{4+}^2$ and $(g_{7/2})_{6+}^2$ neutron configurations. Four-q.p. fully aligned configurations can be obtained by coupling the basic $(g_{9/2})_{8+}^2$ two-q.p. proton configuration with other two-q.p. levels. Studies of these levels may provide further information on the population of the crucial $\nu g_{7/2}$ and $\pi g_{9/2}$ shells. In previous sections, we found that up to $N = 56$ the population of the $\nu g_{7/2}$ shell is low. The low population of the $\nu 1g_{7/2}$ shell at $N = 51$ was also reported in Refs. [62,117]. Interestingly, in a recent study of $^{97}\text{Zr}_{57}$ [35], numerous $7/2^+$ levels are reported, suggesting an increased population of this orbital at $N = 57$.

Figure 22 shows energies of medium-spin positive-parity levels in Sr and Zr isotopes, which correspond to spherical configurations (spin-parity assignments to some of the levels shown are tentative). Figure 22 provides some interesting observations:

(i) Excitation energies are generally lower in Zr nuclei than in their Sr isotones.

(ii) Energies of two- and four-quasiparticle configurations in Sr isotopes decrease with the increasing N .

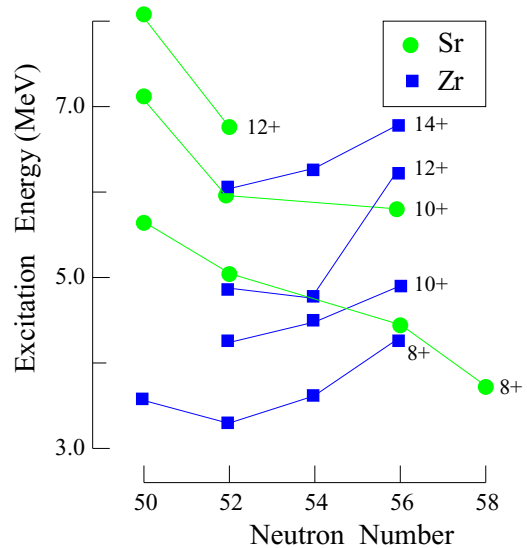


FIG. 22. Experimental excitation energies of medium-spin positive-parity levels in Sr and Zr isotopes. The data are taken from this paper and Refs. [4,116,118].

(iii) In contrast to Sr nuclei the energies in Zr isotopes increase with the increasing N (medium-spin spherical configurations are not known in ^{98}Zr).

Lower excitation energies in Zr isotopes are most likely due to higher population of the $\pi g_{9/2}$ shell in Zr than in Sr nuclei. However, the decrease in the 8^+ energy as a function of the neutron number in Sr isotopes and its increase in Zr isotopes suggest the involvement of neutron levels. The $N = 56$ shell closure at $Z=40$ is stronger than at $Z=38$ (see Fig. 8). Consequently, the population of the $\nu g_{7/2}$ shell may be higher in Sr compared to Zr isotopes. Due to the SOP mechanism the higher population of the $\nu g_{7/2}$ shell may result in lower excitation of the $(g_{9/2})_{8+}^2$ level in Sr nuclei. The strong closure at $N = 56$ in Zr isotopes is responsible for the energy increases seen in Fig. 22. It seems that higher population of the $\pi g_{9/2}$ shell in Zr isotopes, expected to increase the collectivity is not sufficient to override the $Z=40$ shell closure effect.

Finally, let us comment on the high- K 2-q.p. band in ^{96}Sr . In Ref. [48], the (6^+) level at 2533.1 keV in ^{98}Sr was interpreted as the parallel coupling of the $9/2^+[404]$ and $3/2^+[411]$ neutron orbitals. Their (3^+) antiparallel coupling was proposed in ^{98}S at 1837.8 keV [87], defining rather large Gallagher-Moszkowski interaction of 696 keV [48]. The rotational band of $\Delta I = 1$ transitions on top of the 2533.1-keV level in ^{98}Sr is very similar to the band on top of the 3605.4-keV (6^+) level in ^{96}Sr . Assuming the $\nu 9/2^+[404] \otimes 3/2^+[411]$ configuration of the 3605.4-keV level, one may expect the antiparallel 3^+ coupling in ^{96}Sr above 2.9 MeV. Such a level could be populated in the β decay of the 2^+ ground state of ^{96}Rb . A possible candidate is the 3064.8-keV level [51] as suggested by our triple coincidence data, which shows a weak 145-keV feeding of this level.

The 1071-keV drop of the proposed $\nu(9/2^+[404] \otimes 3/2^+[411])_{6+}$ configuration between ^{96}Sr and ^{98}Sr suggests that both orbitals involved are closer to the Fermi surface at

$N = 60$ than at $N = 58$, which coincides with the picture in Figs. 10(d) and 10(e). This supports further the involvement of the $\nu(9/2^+[404])$ extruder in the development of strongly deformed configurations around $N = 60$.

IV. SUMMARY AND PERSPECTIVES

To summarize, excited levels in $^{90-96}\text{Sr}$ were studied using data from measurements of γ rays following spontaneous fission of ^{252}Cf and neutron-induced fission of ^{235}U , performed with Gammasphere and EXILL multidetector arrays, respectively. In total 23 new levels with 30 new or corrected decays and 39 new or improved spin-parity assignments were obtained in these nuclei. In ^{96}Sr , we found the $2_2^+ \rightarrow 0_2^+$, E2 transition in the deformed band and determined its rate of $B(E2) \geq 38(8)\text{W.u.}$ A mechanism involving the $\nu 9/2^+[404]$ extruder was proposed to explain the origin of 0^+ excitations and the evolution of deformation in Sr isotopes. A new classification of 2^+ excitations in the region, supported by the large-scale shell-model calculations (see Fig. 14) was presented, indicating that most of the 2^+ excitations in the studied nuclei are dominated by single-particle excitations, which do not contribute significantly to a development of quadrupole collectivity. These s.-p. excitations provide, how-

ever, a skeleton for other collective excitations, such as γ vibrations and mixed-parity excitations. The latter are now proposed also in Sr isotopes. The LSSM calculations describe well the 3^+ excitations characteristic of these modes. However, the calculation do not reproduce the systematic of 3^- levels in Sr isotopes above $N = 92$, suggesting an admixture of collective effects setting in with the increasing neutron number.

Further experimental studies of Sr isotopes are of high interest. First of all, measurements of nucleon-pair transfer to and from 0_i^+ and 2_i^+ excitations in the $A \approx 100$ region should be performed, to verify their structures proposed in this paper.

ACKNOWLEDGMENTS

We thank the technical services of the ILL, LPSC, and GANIL for supporting the EXILL campaign. The Exogam collaboration and the INFN Legnaro are acknowledged for the loan of Ge detectors. This material is based upon work supported by the US Department of Energy, Office of Science, Office of Nuclear Physics, under Contract No. DE-AC02-06CH11357.

-
- [1] W. Urban, T. Rząca-Urban, J. Wiśniewski, I. Ahmad, A. G. Smith, and G. S. Simpson, *Phys. Rev. C* **99**, 064325 (2019).
 - [2] K. Heyde and J. L. Wood, *Rev. Mod. Phys.* **83**, 1467 (2011).
 - [3] W. Urban, M. Jentschel, R. F. Casten, J. Jolie, C. Bernards, B. Maerkisch, T. Materna, P. Mutti, L. Próchniak, T. Rząca-Urban, G. S. Simpson, V. Werner, and S. Ahmed, *Phys. Rev. C* **87**, 031304(R) (2013).
 - [4] Evaluated Nuclear Structure Data File (ENSDF), www.nndc.bnl.gov/ensdf/.
 - [5] F. Schussler, J. A. Pinston, E. Monnard, A. Moussa, G. Jung, E. Koglin, B. Pfeiffer, R. V. F. Janssens, and J. van Klinken, *Nucl. Phys.* **A339**, 415 (1980).
 - [6] J. F. Sharpey-Schafer, S. M. Mulins, R. A. Bark, J. Kau, F. Komati, E. A. Lawrie, J. J. Lawrie, T. E. Madiba, P. Maine, A. Minkova, S. H. T. Murray, N. J. Ncapayi, and P. A. Vymers, *Eur. Phys. J. A* **47**, 5 (2011).
 - [7] J. F. Sharpey-Schafer, R. A. Bark, S. P. Bvumbi, T. R. S. Dinoko, and S. N. T. Majola, *Eur. Phys. J. A* **55**, 15 (2019).
 - [8] W. Urban, T. Rząca-Urban, A. G. Smith, G. S. Simpson, and J. P. Greene, *Phys. Rev. C* **102**, 064321 (2020).
 - [9] B. R. Mottelson and S. G. Nilsson, *Phys. Rev.* **99**, 1615 (1955).
 - [10] F. Barranco, G. F. Bertsch, R. A. Broglia, and E. Vigezzi, *Nucl. Phys.* **A512**, 253 (1990).
 - [11] R. A. Broglia, F. Barranco, G. F. Bertsch, and E. Vigezzi, *Phys. Rev. C* **49**, 552 (1994).
 - [12] K. Matsuyanagi, M. Matsuo, T. Nakatsukasa, K. Yoshida, N. Hinohara, and K. Sato, *Phys. Scr.* **91**, 063014 (2016).
 - [13] V. Paar, *Nucl. Phys. A* **211**, 29 (1973); *Phys. Lett. B* **39**, 587 (1972).
 - [14] A. Kuriyama, T. Marumori, and K. Matsuyanagi, *Prog. Theor. Phys.* **47**, 498 (1972); **51**, 779 (1974).
 - [15] A. Kuriyama, T. Marumori, K. Matsuyanagi, and R. Okamoto, *Prog. Theor. Phys.* **53**, 489 (1975).
 - [16] T. Rząca-Urban, M. Czerwiński, W. Urban, A. G. Smith, I. Ahmad, F. Nowacki, and K. Sieja, *Phys. Rev. C* **88**, 034302 (2013).
 - [17] J. Wiśniewski, W. Urban, M. Czerwiński, J. Kurpeta, A. Płochocki, M. Pomorski, T. Rząca-Urban, K. Sieja, L. Canete, T. Eronen, S. Geldhof, A. Jokinen, A. Kankainen, I. D. Moore, D. A. Nesterenko, H. Penttilä, I. Pohjalainen, S. Rinta-Antila, A. de Roubin, and M. Vilén, *Phys. Rev. C* **100**, 054331 (2019).
 - [18] T. Rząca-Urban, K. Sieja, W. Urban, F. Nowacki, J. L. Durell, A. G. Smith, and I. Ahmad, *Phys. Rev. C* **79**, 024319 (2009).
 - [19] W. Urban, J. L. Durell, W. R. Phillips, A. G. Smith, M. A. Jones, I. Ahmad, A. R. Barnett, M. Bentaleb, S. J. Dorning, M. J. Leddy, E. Lubkiewicz, L. R. Morss, T. Rząca-Urban, R. A. Sareen, N. Schulz, and B. J. Varley, *Z. Phys. A* **358**, 145 (1997).
 - [20] I.-Y. Lee, *Nucl. Phys. A* **520**, c641 (1990).
 - [21] M. Jentschel, A. Blanc G. de France, U. Köster, S. Leoni, P. Mutti, G. S. Simpson, T. Soldenr, C. Ur, W. Urban (EXILL Collaboration), *J. Instrum.* **12**, P11003 (2017).
 - [22] H. Naidja, F. Nowacki, B. Bounthong, M. Czerwiński, T. Rząca-Urban, T. Rogiński, W. Urban, J. Wiśniewski, K. Sieja, A. G. Smith, J. F. Smith, G. S. Simpson, I. Ahmad, and J. P. Greene, *Phys. Rev. C* **95**, 064303 (2017).
 - [23] W. Urban, A. Abramuk, A. Blanc, M. Czerwiński, G. de France, M. Jentschel, U. Köster, S. Leoni, P. Mutti, T. Rząca-Urban, G. S. Simpson, C. A. Ur, and J. Wiśniewski, *J. Instrum.* (to be published).
 - [24] W. L. Talbert, Jr., F. K. Wohn, L. J. Alquist, and C. L. Duke, *Phys. Rev. C* **23**, 1726 (1981).
 - [25] N. Fotiades, J. A. Cizewski, K. Y. Ding, R. Krücken, J. A. Becker, L. A. Bernstein, K. Hauschild, D. P. McNabb, W.

- Younes, P. Fallon, I. Y. Lee, and O. Macchiavelli, *Phys. Scr.* **2000**, 127 (2000).
- [26] E. A. Stefanova, R. Schwengner, G. Rainovski, K. D. Schilling, A. Wagner, F. Donau, E. Galindo, A. Jungclaus, K. P. Lieb, O. Thelen, J. Eberth, D. R. Napoli, C. A. Ur, G. de Angelis, M. Axiotis, A. Gadea, N. Marginean, T. Martinez, T. Kroll, and T. Kutsarova, *Phys. Rev. C* **63**, 064315 (2001).
- [27] S. K. Basu and E. A. McCutchan, *Nucl. Data Sheets* **165**, 1 (2020).
- [28] C. M. Baglin, *Nucl. Data Sheets* **113**, 2187 (2012).
- [29] I. Ahmad and W. R. Phillips, *Rep. Prog. Phys.* **58**, 1415 (1995).
- [30] A. Kumar and M. R. Guynes, *Phys. Rev. C* **32**, 2116 (1985).
- [31] J. Dobaczewski, in *Proceedings of the International Conference on Nuclear Structure Physics, Cocoyoc*, edited by R. Casten, A. Frank, and M. Moshinski (World Scientific, Singapore, 1988), pp. 227–242.
- [32] J. Skalski, P.-H. Heenen, and P. Bonche, *Nucl. Phys. A* **559**, 221 (1993).
- [33] W. Urban, J. L. Durell, A. G. Smith, W. R. Phillips, M. A. Jones, B. J. Varley, T. Rza-Urban, I. Ahmad, L. R. Morss, M. Bentaleb, and N. Schulz, *Nucl. Phys. A* **689**, 605 (2001).
- [34] T. R. Werner, J. Dobaczewski, M. W. Guidry, W. Nazarewicz, and J. A. Sheikh, *Nucl. Phys. A* **578**, 1 (1994).
- [35] T. Rza-Urban, W. Urban, M. Czerwiński, J. Wiśniewski, A. Blanc, H. Faust, M. Jentschel, P. Mutti, U. Köster, T. Soldner, G. de France, G. S. Simpson, and C. A. Ur, *Phys. Rev. C* **98**, 064315 (2018).
- [36] J. H. Hamilton, A. V. Ramayya, S. J. Zhu, G. M. Ter-Akopian, Y. T. Oganessian, J. D. Cole, J. O. Rasmussen, and M. A. Stoyer, *Prog. Nucl. Part. Phys.* **35**, 635 (1995).
- [37] J.-M. Régis, J. Jolie, N. Saed-Samii, N. Warr, M. Pfeiffer, A. Blanc, M. Jentschel, U. Köster, P. Mutti, T. Soldner, G. S. Simpson, F. Drouet, A. Vancraeynest, G. de France, E. Clément, O. Stezowski, C. A. Ur, W. Urban, P. H. Regan, Zs. Podolyák, C. Larijani, C. Townsley, R. Carroll, E. Wilson, L. M. Fraile, H. Mach, V. Pazyi, B. Olaizola, V. Vedia, A. M. Bruce, O. J. Roberts, J. F. Smith, M. Scheck, T. Kröll, A.-L. Hartig, A. Ignatov, S. Ilieva, S. Lalkovski, W. Korten, N. Marginean, T. Otsuka, N. Shimizu, T. Togashi, and Y. Tsunoda, *Phys. Rev. C* **95**, 054319 (2017).
- [38] G. Jung, B. Pfeiffer, L. J. Alquist, H. Wollnik, P. Hungerford, S. M. Scott, and W. D. Hamilton, *Phys. Rev. C* **22**, 252 (1980).
- [39] A. Negret, and A. A. Sonzogni, Evaluated Nuclear Structure Data File (2011).
- [40] I. Tsekhanovich, G. S. Simpson, W. Urban, J. A. Dare, J. Jolie, A. Linnemann, R. Orlandi, A. Scherillo, A. G. Smith, T. Soldner, B. J. Varley, T. Rza-Urban, A. Złomanić, O. Dorvaux, B. J. P. Gall, B. Roux, and J. F. Smith, *Phys. Rev. C* **78**, 011301(R) (2008).
- [41] S. Cruz, K. Wimmer, S. S. Bhattacharjee, P. C. Bender, G. Hackman, R. Krucken, F. Ames, C. Andreoiu, R. A. E. Austin, C. S. Bancroft *et al.*, *Phys. Rev. C* **102**, 024335 (2020).
- [42] G. Jung, Nuclear Spectroscopy on Neutron Rich Rubidium With Even Mass Numbers, Ph.D. thesis, Justus Liebig-Universität, Giessen, 1980.
- [43] E. Clément, M. Zielińska, A. Gørgen, W. Korten, S. Péru, J. Libert, H. Goutte, S. Hilaire, B. Bastin, C. Bauer *et al.*, *Phys. Rev. Lett.* **116**, 022701 (2016).
- [44] E. Clément, M. Zielińska, S. Péru, H. Goutte, S. Hilaire, A. Gørgen, W. Korten, D. T. Doherty, B. Bastin, C. Bauer *et al.*, *Phys. Rev. C* **94**, 054326 (2016).
- [45] S. Cruz, P. C. Bender, R. Krucken, K. Wimmer, F. Ames, C. Andreoiu, R. A. E. Austin, C. S. Bancroft, R. Braid, T. Bruhn *et al.*, *Phys. Lett. B* **786**, 94 (2018).
- [46] S. Cruz, K. Wimmer, P. C. Bender, R. Krucken, G. Hackman, F. Ames, C. Andreoiu, R. A. E. Austin, C. S. Bancroft, R. Braid *et al.*, *Phys. Rev. C* **100**, 054321 (2019).
- [47] M. A. C. Hotchkis, J. L. Durell, J. B. Fitzgerald, A. S. Mowbray, W. R. Phillips, I. Ahmad, M. P. Carpenter, R. V. F. Janssens, T. L. Khoo, E. F. Moore, L. R. Morss, Ph. Benet, and D. Ye, *Nucl. Phys. A* **530**, 111 (1991).
- [48] J. L. Durell, T. J. Armstrong, and W. Urban, *Eur. Phys. J. A* **20**, 97 (2004).
- [49] A. G. Smith, J. L. Durell, W. R. Phillips, W. Urban, P. Sarriguren, and I. Ahmad, *Phys. Rev. C* **86**, 014321 (2012).
- [50] C. Y. Wu, H. Hua, D. Cline, A. B. Hayes, R. Teng, R. M. Clark, P. Fallon, A. Goergen, A. O. Macchiavelli, and K. Vetter, *Phys. Rev. C* **70**, 064312 (2004).
- [51] D. Abriola and A. A. Sonzogni, *Nucl. Data Sheets* **109**, 2501 (2008).
- [52] P. Federman and S. Pittel, *Phys. Lett. B* **69**, 385 (1977); **77**, 29 (1978); *Phys. Rev. C* **20**, 820 (1979).
- [53] C. Kremer, S. Aslanidou, S. Bassauer, M. Hilcker, A. Krugmann, P. von Neumann-Cosel, T. Otsuka, N. Pietralla, V. Y. Ponomarev, N. Shimizu, M. Singer, G. Steinhilber, T. Togashi, Y. Tsunoda, V. Werner, and M. Zweidinger, *Phys. Rev. Lett.* **117**, 172503 (2016).
- [54] Y. Tsunoda, T. Otsuka, N. Shimizu, M. Honma, and Y. Utsuno, *Phys. Rev. C* **89**, 031301(R) (2014).
- [55] R. A. Meyer, E. Monnard, J. A. Pinston, F. Schussler, B. Pfeiffer, I. Ragnarsson, H. Lawin, G. Lhersonneau, and K. Sistemich, *Nucl. Phys. A* **439**, 510 (1985).
- [56] B. M. Nyakó, J. Timár, M. Csatlós, Zs. Dombrádi, A. Krasznahorkay, I. Kuti, D. Sohler, T. G. Tornyi, M. Czerwiński, T. Rza-Urban, W. Urban, P. Bączyk, L. Atanasova, D. L. Balabanski, K. Sieja, A. Blanc, M. Jentschel, U. Köster, P. Mutti, T. Soldner, G. de France, G. S. Simpson *et al.*, *Phys. Rev. C* **103**, 034304 (2021).
- [57] W. Urban, K. Sieja, T. Materna, M. Czerwiński, T. Rza-Urban, A. Blanc, M. Jentschel, P. Mutti, U. Köster, T. Soldner, G. de France, G. S. Simpson, C. A. Ur, C. Bernards, C. Fransen, J. Jolie, J.-M. Régis, T. Thomas, and N. Warr, *Phys. Rev. C* **94**, 044328 (2016).
- [58] K. Heyde, P. Van Isacker, R. F. Casten, and J. L. Wood, *Phys. Lett. B* **155**, 303 (1985).
- [59] W. Urban, T. Rza-Urban, A. Złomanić, G. Simpson, J. L. Durell, W. R. Phillips, A. G. Smith, B. J. Varley, I. Ahmad, and N. Schulz, *Eur. Phys. J. A* **16**, 11 (2003).
- [60] W. Urban, J. A. Pinston, J. Genevey, T. Rza-Urban, A. Złomanić, G. Simpson, J. L. Durell, W. R. Phillips, A. G. Smith, B. J. Varley, I. Ahmad, and N. Schulz, *Eur. Phys. J. A* **22**, 241 (2004).
- [61] K. Sieja, F. Nowacki, K. Langanke, and G. Martinez-Pinedo, *Phys. Rev. C* **79**, 064310 (2009).
- [62] F. Didierjean, D. Verney, G. Duchêne, J. Litzinger, K. Sieja, A. Dewald, A. Goasduff, R. Lozeva, C. Fransen, G. deAngelis, S. Aydin, D. Bazzacco, A. Bracco, S. Bottoni, L. Corradi, F. Crespi, E. Ellinger, E. Farnea, E. Fioretto, S. Franchoo, A. Gottardo, L. Grocutt, M. Hackstein, F. Ibrahim, K. Kolos, S. Leoni, S. Lenzi, S. Lunardi, R. Menegazzo, D. Mengoni, C. Michelagnoli, T. Mijatovic, V. Modamio, O. Möller, G. Montagnoli, D. Montanari, A. I. Morales, D. Napoli, M.

- Niikura, F. Recchia, E. Sahin, F. Scarlassara, L. Sengele, S. Szilner, J. F. Smith, A. M. Stefanini, C. Ur, J. J. Valiente-Dobón, and V. Vandone, *Phys. Rev. C* **96**, 044320 (2017).
- [63] T. Materna, W. Urban, K. Sieja, U. Köster, H. Faust, M. Czerwiński, T. Rząca-Urban, C. Bernards, C. Fransen, J. Jolie, J.-M. Regis, T. Thomas, and N. Warr, *Phys. Rev. C* **92**, 034305 (2015).
- [64] T. Rząca-Urban, K. Sieja, W. Urban, M. Czerwiński, A. Blanc, M. Jentschel, P. Mutti, U. Köster, T. Soldner, G. de France, G. S. Simpson, and C. A. Ur, *Phys. Rev. C* **95**, 064302 (2017).
- [65] K. Sieja (unpublished).
- [66] F. Buchinger, E. B. Ramsay, E. Arnold, W. Neu, R. Neugart, K. Wendt, R. E. Silverans, P. Lievens, L. Vermeeren, D. Berdichevsky, R. Fleming, D. W. L. Sprung, and G. Ulm, *Phys. Rev. C* **41**, 2883 (1990); **42**, 2754(E) (1990).
- [67] N. Gavriyelov, A. Leviatan, and F. Iachello, *Phys. Rev. C* **99**, 064324 (2019).
- [68] J. E. Garcia-Ramos and K. Heyde, *Phys. Rev. C* **100**, 044315 (2019).
- [69] P. E. Garrett, *J. Phys. G: Nucl. Part. Phys.* **27**, R1 (2001).
- [70] P. E. Garrett, W. D. Kulp, J. L. Wood, D. Bandyopadhyay, S. Choudry, D. Dashdorj, S. R. Leshner, M. T. McEllistrem, M. Mynk, J. N. Orce, and S. W. Yates, *Phys. Rev. Lett.* **103**, 062501 (2009).
- [71] A. Leviatan, N. Gavriyelov, J. E. Garcia-Ramos, and P. Van Isacker, *Phys. Rev. C* **98**, 031302(R) (2018).
- [72] T. Togashi, Y. Tsunoda, T. Otsuka, and N. Shimizu, *Phys. Rev. Lett.* **117**, 172502 (2016).
- [73] P. E. Garrett, L. Makhathini, R. A. Bark, T. R. Rodriguez, S. Valbuena, V. Bildstein, T. D. Bucher, C. Burbadge, R. Dubey, T. Faestermann *et al.*, *Phys. Lett. B* **809**, 135762 (2020).
- [74] G. F. Bertsch, *Eur. Phys. J. A* **55**, 248 (2019).
- [75] P. F. Bortignon, and R. A. Broglia, *Eur. Phys. J. A* **52**, 280 (2016).
- [76] C. Walz, H. Fujita, A. Krugmann, P. von Neumann-Cosel, N. Pietralla, V. Y. Ponomarev, A. Scheikh-Obeid, and J. Wambach, *Phys. Rev. Lett.* **106**, 062501 (2011).
- [77] B. Elman, A. Gade, D. Weisshaar, D. Barofsky, D. Bazin, P. C. Bender, M. Bowry, M. Hjorth-Jensen, K. W. Kemper, S. Lipschutz, E. Lunderberg, N. Sachmpazidi, N. Terpstra, W. B. Walters, A. Westerberg, S. J. Williams, and K. Wimmer, *Phys. Rev. C* **96**, 044332 (2017).
- [78] A. Chester, G. C. Ball, R. Caballero-Folch, D. S. Cross, S. Cruz, T. Domingo, T. E. Drake, A. B. Garnsworthy, G. Hackman, S. Hallam, J. Henderson, R. Henderson, W. Korten, R. Krucken, M. Moukaddam, B. Olaizola, P. Ruotsalainen, J. Smallcombe, K. Starosta, C. E. Svensson, J. Williams, and K. Wimmer, *Phys. Rev. C* **96**, 011302(R) (2017).
- [79] J. Dudouet, A. Lemasson, G. Duchene, M. Rejmund, E. Clement, C. Michelagnoli, F. Didierjean, A. Korichi, G. Maquart, O. Stezowski, C. Lizarazo *et al.*, *Phys. Rev. Lett.* **118**, 162501 (2017).
- [80] K. Heyde, J. Jolie, R. Fossion, S. De Baerdemacker, and V. Hellemans, *Phys. Rev. C* **69**, 054304 (2004).
- [81] R. F. Casten and E. A. McCutchan, *J. Phys. G: Nucl. Part. Phys.* **34**, R285 (2007).
- [82] S. Naimi, G. Audi, D. Beck, K. Blaum, C. Böhm, C. Borgmann, M. Breitenfeldt, S. George, F. Herfurth, A. Herlert, M. Kowalska, S. Kreim, D. Lunney, D. Neidherr, M. Rosenbusch, S. Schwarz, L. Schweikhard, and K. Zuber, *Phys. Rev. Lett.* **105**, 032502 (2010).
- [83] I. Mukul, C. Andreoiu, J. Bergmann, M. Brodeur, T. Brunner, K. A. Dietrich, T. Dickel, I. Dillmann, E. Dunling, D. Fusco, G. Gwinner, C. Izzo, A. Jacobs, B. Kootte, Y. Lan, E. Leitschneider, E. M. Lykiardopoulou, S. F. Paul, M. P. Reiter, J. L. Tracy, Jr., J. Dilling, and A. A. Kwiatkowski, *Phys. Rev. C* **103**, 044320 (2021).
- [84] R. B. Cakirli, R. F. Casten, R. Winkler, K. Blaum, and M. Kowalska, *Phys. Rev. Lett.* **102**, 082501 (2009).
- [85] R. B. Cakirli, R. F. Casten, and K. Blaum, *Phys. Rev. C* **82**, 061306(R) (2010).
- [86] R. Rodriguez-Guzman, P. Sarriguren, L. M. Robledo, and S. Perez-Martin, *Phys. Lett. B* **691**, 202 (2010).
- [87] G. Lhersonneau, B. Pfeiffer, R. Capote, J. M. Quesada, H. Gabelmann, K.-L. Kratz, and the ISOLDE Collaboration, *Phys. Rev. C* **65**, 024318 (2002).
- [88] J. K. Hwang, A. V. Ramayya, J. H. Hamilton, D. Fong, C. J. Beyer, P. M. Gore, Y. X. Luo, J. O. Rasmussen, S. C. Wu, I. Y. Lee, C. M. Folden III, P. Fallon, P. Zielinski, K. E. Gregorich, A. O. Macchiavelli, M. A. Stoyer, S. J. Asztalos, T. N. Ginter, S. J. Zhu, J. D. Cole, G. M. Ter Akopian, Y. T. Oganessian, and R. Donangelo, *Phys. Rev. C* **67**, 054304 (2003).
- [89] A. Złomaniec, H. Faust, J. Genevey, J. A. Pinston, T. Rząca-Urban, G. S. Simpson, I. Tsekhanovich, and W. Urban, *Phys. Rev. C* **72**, 067302 (2005).
- [90] W. Urban, M. Czerwiński, J. Kurpeta, T. Rząca-Urban, J. Wiśniewski, T. Materna, Ł. W. Iskra, A. G. Smith, I. Ahmad, A. Blanc, H. Faust, U. Köster, M. Jentschel, P. Mutti, T. Soldner, G. S. Simpson, J. A. Pinston, G. de France, C. A. Ur, V.-V. Elomaa, T. Eronen, J. Hakala, A. Jokinen, A. Kankainen, I. D. Moore, J. Rissanen, A. Saastamoinen, J. Szerypo, C. Weber, and J. Äystö, *Phys. Rev. C* **96**, 044333 (2017).
- [91] A. Esmaylzadeh, J.-M. Regis, Y. H. Kim, U. Köster, J. Jolie, V. Karayonchev, L. Knafla, K. Nomura, L. M. Robledo, and R. Rodriguez-Guzman, *Phys. Rev. C* **100**, 064309 (2019).
- [92] A. Guessous, N. Schulz, M. Bentaleb, E. Lubkiewicz, J. L. Durell, C. J. Pearson, W. R. Phillips, J. A. Shannon, W. Urban, B. J. Varley, I. Ahmad, C. J. Lister, L. R. Morss, K. L. Nash, C. W. Williams, and S. Khazrouni, *Phys. Rev. C* **53**, 1191 (1996).
- [93] J. A. Shannon, W. R. Phillips, J. L. Durell, B. J. Varley, W. Urban, C. J. Pearson, I. Ahmad, C. J. Lister, L. R. Morss, K. L. Nash, C. W. Williams, N. Schulz, E. Lubkiewicz, and M. Bentaleb, *Phys. Lett. B* **336**, 136 (1994).
- [94] A. Guessous, N. Schulz, W. R. Phillips, I. Ahmad, M. Bentaleb, J. L. Durell, M. A. Jones, M. Leddy, E. Lubkiewicz, L. R. Morss, R. Piepenbring, A. G. Smith, W. Urban, and B. J. Varley, *Phys. Rev. Lett.* **75**, 2280 (1995).
- [95] N. V. Zamfir and R. F. Casten, *Phys. Lett. B* **260**, 265 (1991).
- [96] E. A. McCutchan, D. Bonatsos, N. V. Zamfir, and R. F. Casten, *Phys. Rev. C* **76**, 024306 (2007).
- [97] R. F. Casten, R. B. Cakirli, D. Bonatsos, and K. Blaum, *Phys. Rev. C* **102**, 054310 (2020).
- [98] A. Poves, F. Nowacki, and Y. Alhassid, *Phys. Rev. C* **101**, 054307 (2020).
- [99] I. N. Gratchev, G. S. Simpson, G. Thiamova, M. Ramdhane, K. Sieja, A. Blanc, M. Jentschel, U. Koster, P. Mutti, T. Soldner, G. deFrance, C. A. Ur, and W. Urban, *Phys. Rev. C* **95**, 051302(R) (2017).
- [100] W. Urban, T. Rząca-Urban, J. Wiśniewski, A. G. Smith, G. S. Simpson, and I. Ahmad, *Phys. Rev. C* **100**, 014319 (2019).

- [101] K. Sieja, T. R. Rodriguez, K. Kolos, and D. Verney, *Phys. Rev. C* **88**, 034327 (2013).
- [102] S. W. Yates, *J. Radiol. Nucl. Chem.* **265**, 291 (2005).
- [103] N. Pietralla, P. von Brentano, and A. F. Lisetskiy, *Prog. Part. Nucl. Phys.* **60**, 225 (2008).
- [104] K. Sieja, G. Martinez-Pinedo, L. Coquard, and N. Pietralla, *Phys. Rev. C* **80**, 054311 (2009).
- [105] V. Werner, D. Belic, P. von Brentano, C. Fransen, A. Gade, H. von Garrel, J. Jolie, U. Kneissl, C. Kohstall, A. Linnemann, A. F. Lisetskiy, N. Pietralla, H. H. Pitz, M. Sheck, K.-H. Speidel, F. Stedile, and S. W. Yates, *Phys. Lett. B* **550**, 140 (2002).
- [106] N. Pietralla, C. Fransen, D. Belic, P. von Brentano, C. Frießner, U. Kneissl, A. Linnemann, A. Nord, H. H. Pitz, T. Otsuka, I. Schneider, V. Werner, and I. Wiedenhöver, *Phys. Rev. Lett.* **83**, 1303 (1999).
- [107] N. Pietralla, C. Fransen, P. von Brentano, A. Dewald, A. Fitzler, C. Frießner, and J. Gableske, *Phys. Rev. Lett.* **84**, 3775 (2000).
- [108] C. Fransen, N. Pietralla, P. von Brentano, A. Dewald, J. Gableske, A. Gade, A. Lisetskiy, and V. Werner, *Phys. Lett. B* **508**, 219 (2001).
- [109] C. Fransen, N. Pietralla, Z. Ammar, D. Bandyopadhyay, N. Boukharouba, P. von Brentano, A. Dewald, J. Gableske, A. Gade, J. Jolie, U. Kneissl, S. R. Leshner, A. F. Lisetskiy, M. T. McEllistrem, M. Merrick, H. H. Pitz, N. Warr, V. Werner, and S. W. Yates, *Phys. Rev. C* **67**, 024307 (2003).
- [110] T. Thomas, V. Werner, J. Jolie, K. Nomura, T. Ahn, N. Cooper, H. Duckwitz, A. Fitzler, C. Fransen, A. Gade *et al.*, *Nucl. Phys. A* **947**, 203 (2016).
- [111] H. Klein, A. F. Lisetskiy, N. Pietralla, C. Fransen, A. Gade, and P. von Brentano, *Phys. Rev. C* **65**, 044315 (2002).
- [112] K. Heyde, P. von Neumann-Cosel, and A. Richter, *Rev. Mod. Phys.* **82**, 2365 (2010).
- [113] E. A. McCutchan and A. A. Sonzogni, *Nucl. Data Sheets* **115**, 135 (2014).
- [114] T. Rzača-Urban, W. Urban, A. Kaczor, J. L. Durell, M. J. Leddy, M. A. Jones, W. R. Phillips, A. G. Smith, B. J. Varley, I. Ahmad, L. R. Morss, M. Bentalib, E. Lubkiewicz, and N. Schulz, *Eur. Phys. J. A* **9**, 165 (2000).
- [115] E. T. Gregor, N. N. Arsenyev, M. Scheck, T. M. Shneidman, M. Thurauf, C. Bernardis, A. Blanc, R. Chapman, F. Drouet, A. A. Dzhioev *et al.*, *J. Phys. G: Nucl. Part. Phys.* **46**, 075101 (2019).
- [116] G. S. Simpson, J. A. Pinston, D. Balabanski, J. Genevey, G. Georgiev, J. Jolie, D. S. Judson, R. Orlandi, A. Scherillo, I. Tsekhanovich, W. Urban, and N. Warr, *Phys. Rev. C* **74**, 064308 (2006).
- [117] D. K. Sharp, B. P. Kay, J. S. Thomas, S. J. Freeman, J. P. Schiffer, B. B. Back, S. Bedoor, T. Bloxham, J. A. Clark, C. M. Deibel, C. R. Hoffman, A. M. Howard, J. C. Lighthall, S. T. Marley, A. J. Mitchell, T. Otsuka, P. D. Parker, K. E. Rehm, D. V. Shetty, and A. H. Wuosmaa, *Phys. Rev. C* **87**, 014312 (2013).
- [118] D. Pantelica, I. G. Stefan, N. Nica, M.-G. Porquet, G. Duchêne, A. Astier, S. Courtin, I. Deloncle, F. Hoellinger, A. Bauchet, N. Bufor, L. Donadille, O. Dorvaux, J. Duprat, B. J.P. Gall, C. Gautherin, T. Kutsarova, S. Lalkovski, R. Lucas, M. Meyer, A. Minkova, A. Prevost, N. Redon, N. Schulz, H. Sergolle, O. Stężowski, T. Venkova, and A. Wilson, *Phys. Rev. C* **72**, 024304 (2005).